REGENERATION

Alcaligenes faecalis corrects aberrant matrix metalloproteinase expression to promote reepithelialization of diabetic wounds

Ellen K. White[1], Aayushi Uberoi[1], Jamie Ting-Chun Pan[1], Jordan T. Ort[1], Amy E. Campbell[1], Sofia M. Murga-Garrido[1], Jordan C. Harris[1], Preeti Bhanap[1], Monica Wei[1], Nelida Y. Robles[1], Sue E. Gardner[2], Elizabeth A. Grice[1]*

Chronic wounds are a common and costly complication of diabetes, where multifactorial defects contribute to dysregulated skin repair, inflammation, tissue damage, and infection. We previously showed that aspects of the diabetic foot ulcer microbiota were correlated with poor healing outcomes, but many microbial species recovered remain uninvestigated with respect to wound healing. Here, we focused on *Alcaligenes faecalis*, a Gram-negative bacterium that is frequently recovered from chronic wounds but rarely causes infection. Treatment of diabetic wounds with *A. faecalis* accelerated healing during early stages. We investigated the underlying mechanisms and found that *A. faecalis* treatment promotes reepithelialization of diabetic keratinocytes, a process that is necessary for healing but deficient in chronic wounds. Overexpression of matrix metalloproteinases in diabetes contributes to failed epithelialization, and we found that *A. faecalis* treatment balances this overexpression to allow proper healing. This work uncovers a mechanism of bacterial-driven wound repair and provides a foundation for the development of microbiota-based wound interventions.

INTRODUCTION

Skin injury occurs in the context of microbial communities, which can subsequently contaminate and colonize injured tissue. The "wound microbiome" is a ubiquitous component of the wound environment and has been associated with healing outcomes (*1*–*3*). Considered a silent epidemic, chronic wounds affect over 6 million people in the United States each year (*4*). As the number of people with chronic wounds increases, health care costs also surge, with recent estimates of 96 billion spent annually on management of nonhealing wounds (*5*). In addition, patients with chronic wounds experience pain, morbidity, immobility, and even social isolation (*6*–*9*). Given this mounting health care threat, there is an unmet need for improved, personalized therapies that target molecular mechanisms specific to wound pathophysiology (*10*). The wound microbiota and its mechanisms of interacting with host cells during repair represent a promising source of previously unidentified therapeutic targets and/or disease biomarkers.

There is growing evidence that resident skin microbes promote several components of the host skin repair and wound healing responses (*11*). Skin commensal bacteria can promote epithelialization and barrier function by regulating the keratinocyte aryl hydrocarbon receptor (*12*, *13*). Commensal bacteria can modulate the inflammatory cascade needed for proper repair and regeneration of wounded skin (*14*–*16*). Immune cells that are specific to commensal bacteria are recruited after tissue damage and can promote injury repair (*17*–*20*). Colonizing skin bacteria have also been shown to promote cutaneous nerve regeneration after injury (*21*). These processes of inflammatory cytokine signaling, immune cell recruitment, epithelialization, and regeneration are dysregulated in chronic wounds. In addition, dysregulated inflammation, disorganized keratinocyte function, and increased peptidase activity contribute to the wound healing impairment in diabetic skin (*22*). Given the role of skin microbes in promoting diverse tissue repair mechanisms, we hypothesized that microbial-driven responses could be leveraged to correct these dysfunction processes that lead to nonhealing wounds.

The risk of infection as well as an incomplete understanding of the wound microbiome has led to clinical practices that seek to eradicate wound microbes. Community-wide culture-independent profiling of the wound microbiota has provided a more comprehensive, less-biased understanding of microbes that are present, as well as their dynamics during healing and complications (*2*, *3*, *23*). Although well-characterized wound pathogens such as *Staphylococcus aureus* and *Pseudomonas aeruginosa* are commonly detected by these methods, these pathogens do not exist in isolation but in communities with other microbes that are poorly characterized in the context of cutaneous wounds. We previously conducted shotgun metagenomic sequencing of 195 samples collected from 46 diabetic foot ulcers (DFUs), and by rank mean abundance, *S. aureus* and *P. aeruginosa* were the top taxa detected, followed by *Corynebacterium striatum*, *Propionibacterium* species, and *Alcaligenes faecalis* (*24*). *C. striatum* and *Propionibacterium* spp. are considered human skin commensals, while *A. faecalis* is considered a nonpathogenic environmental bacterium (*25*).

Because commensal microbes can promote many cutaneous repair processes, our objective was to examine the role of wound colonizers and to identify mechanisms of microbial-host cross-talk that contribute to healing outcomes. Here, we investigated *A. faecalis*, a Gram-negative rod that is frequently recovered from chronic wounds by both culture-dependent and culture-independent methods. While shotgun metagenomic sequencing indicated that *A. faecalis* was the fifth most abundant species, it was not associated with clinical outcomes in our DFU cohort. In a murine diabetic wound healing model, we found that *A. faecalis* treatment promoted early wound healing while colonizing the wound bed. *A. faecalis* culture supernatants induced a proepithelialization phenotype in diabetic keratinocytes, enhancing migration and proliferation. *A. faecalis* induces this prohealing phenotype through modulation

[1]Department of Dermatology, Perelman School of Medicine, University of Pennsylvania, Philadelphia, PA 19104, USA. [2]College of Nursing, The University of Iowa, Iowa City, IA 52242, USA.
*Corresponding author. Email: egrice@pennmedicine.upenn.edu

of matrix metalloproteinase (MMP) pathways, which are overactive in diabetes and contribute to the highly proteolytic environment that is detrimental to wound healing (*26*–*32*). Thus, we uncover a previously unidentified mechanism by which a member of the wound microbiome can promote skin repair and wound healing.

RESULTS

A. faecalis is a common member of the chronic wound microbiota and promotes early wound closure in a murine diabetic model

We previously identified *A. faecalis* as a prevalent and abundant member of the DFU microbiome, through both culture-dependent and culture-independent methods (*24*). In a longitudinal prospective cohort study of 100 DFUs, we performed quantitative cultures in parallel with culture-independent methods to identify microbial bioburden associated with clinical outcomes (Fig. 1A). Cultures identified 44 *A. faecalis* isolates from 14 DFUs (Fig. 1B). Shotgun metagenomic sequencing indicated that *A. faecalis* comprised up to 38% mean relative abundance in culture-positive DFUs (Fig. 1B). Although *A. faecalis* was ranked 5th by mean relative abundance overall, we did not find an association with DFU outcome in our analysis (*24*). Our findings are supported by additional studies where *Alcaligenes* is consistently identified in chronic wounds other than DFUs, including pressure ulcers (PUs), venous leg ulcers (VLUs), and sickle cell disease leg ulcers (SCLUs) (Table 1) (*33*–*40*).

Despite the lack of association with clinical outcomes, the abundance and prevalence of *A. faecalis* in our cohort motivated us to study the direct impact of *A. faecalis* on diabetic wound healing. To test this, we used a 12-week-old *db/db* diabetic mouse model [B6.BKS(D)-*Lepr*$^{db/db}$], which has demonstrated wound healing defects (*41*). We made full-thickness excisional 8-mm wounds on the shaved mouse dorsum, treated each wound with 2×10^8 colony-forming unit (CFU) of a clinical *A. faecalis* isolate or vehicle control, and covered wounds with Tegaderm. Wounds were photographed, and wound area was measured at days 0, 3, 7, 14, and 21 (Fig. 1C; unedited wound images in fig. S1A). *A. faecalis* colonization significantly accelerated wound closure at day 3 compared to vehicle-treated control (Fig. 1, C and D; $P = 0.015$ by Wilcoxon rank sum test). The *A. faecalis*–treated wounds showed no overt signs of infection and maintain well-defined wound margins (Fig. 1C). The wound bed appeared healthy despite *A. faecalis* colonization persisting at ~2×10^7 CFU at day 3 (Fig. 1E). Inflammatory responses during healing promote clearance of bacteria from the wound bed; partial clearance of *A. faecalis* occurs by day 7 and, by day 14, is completely cleared (Fig. 1E). Thus, *A. faecalis* colonized the wound bed in parallel to enhanced wound closure during early stages but does not persist through later stages.

These results of *A. faecalis* treatment are in contrast to treatment of wounds with *S. aureus*, a well-established wound pathogen (*42*). Using the same inoculum of a *S. aureus* clinical isolate that delayed healing in diabetic wounds (*43*), wound areas at day 3 were significantly enlarged compared to both vehicle- and *A. faecalis*–treated mice (fig. S1B; $*P \leq 0.05$; $**P \leq 0.01$; $****P \leq 0.0001$ by Wilcoxon rank sum test). Despite this dichotomous wound healing response, these two bacteria persisted at similar CFU on day 3 after wounding (fig. S1C; not significant by Wilcoxon rank sum test). Furthermore, at day 3, *S. aureus*–treated wounds have overt signs of inflammation, including erythema, purulent discharge, and macerated wound edges (fig. S1C). Unlike *A. faecalis*, *S. aureus* is not successfully cleared from the wounds, and these wounds do not heal by the day 21 experimental endpoint (fig. S1D). These results indicate that, unlike pathogenic bacteria, *A. faecalis* can promote early wound closure. Therefore, we sought to understand the mechanisms that underlie this microbially mediated wound closure.

A. faecalis improves the epithelialization potential of diabetic keratinocytes

We observed that the strongest effect of *A. faecalis* treatment occurred in the early stages of wound healing, where the critical process of reepithelialization is initiated. During this stage of healing, the wound transitions from the inflammatory phase to proliferative phase, and thus we focus on day 3 as an early wounding time point for several subsequent readouts. Successful wound closure is definitionally dependent on restoration of the epidermis or reepithelialization (*44*). Chronic wounds, including DFUs, are deficient in reepithelialization as well as the processes of keratinocyte migration and proliferation (*44*–*48*). For these reasons, we investigated the effect of *A. faecalis* on reepithelialization.

Migration by wound edge keratinocytes is required to close the gap in epithelia that is created by tissue damage and wounding. To examine keratinocyte migration, we modified an in vitro scratch wound closure assay to use primary diabetic keratinocytes derived from *db/db* mouse epidermis. Confluent cells were treated with 10% sterile-filtered bacterial conditioned media after creating a "scratch" by removing two-well tissue culture inserts. Cells were imaged to measure the initial gap and again after 24 hours. *A. faecalis* conditioned media significantly accelerated keratinocyte migration and closed the gap compared to the untreated control (Fig. 2A; $**P \leq 0.01$ by Wilcoxon test). In contrast, cells treated with the same dose of *S. aureus* conditioned media had no change in migration compared to untreated control. These differences are not due to changes in keratinocyte viability after 24-hour incubation with the bacterial conditioned media (fig. S2A).

In addition to migration, keratinocytes must also proliferate to replace the damaged epithelia. To examine the effect on keratinocyte proliferation, we wounded *db/db* mice and treated wounds with *A. faecalis* or placebo as described above. At 3 days after wounding, mice were pulsed with 5-ethynyl-2′-deoxyuridine (EdU), which labels nascent DNA, for 1 hour before euthanasia and wound harvest. Wounds were sectioned and immunostained for cytokeratin 14 (K14) to mark basal keratinocytes and stained with 4′,6-diamidino-2-phenylindole (DAPI) to mark nuclei. The percent of EdU^+ $K14^+$ epithelial cells was determined and compared (Fig. 2B). *A. faecalis* treatment significantly increased the percentage of proliferating basal keratinocytes at the wound edge compared to phosphate-buffered saline (PBS)–treated control wounds ($*P \leq 0.05$ by Wilcoxon test). Thus, *A. faecalis* also promotes proliferation of basal keratinocytes in vivo in diabetic wounds.

Keratinocyte outgrowth from skin biopsies is an established ex vivo method to assess reepithelialization potential and mimics the properties of migration and proliferation exhibited by wound edge keratinocytes (*49*). To test if *A. faecalis* influences the epithelialization potential of human diabetic skin, we obtained discarded skin from surgery patients with a diabetes diagnosis. Biopsies were created and cultured in 10% *A. faecalis* conditioned media or media alone for 10 days, and keratinocyte outgrowth was quantified. Explants treated with *A. faecalis* conditioned media resulted in significantly larger area of keratinocyte outgrowth ($*P \leq 0.05$ by Wilcoxon test) compared to vehicle control (Fig. 2C). Together, these findings demonstrate that

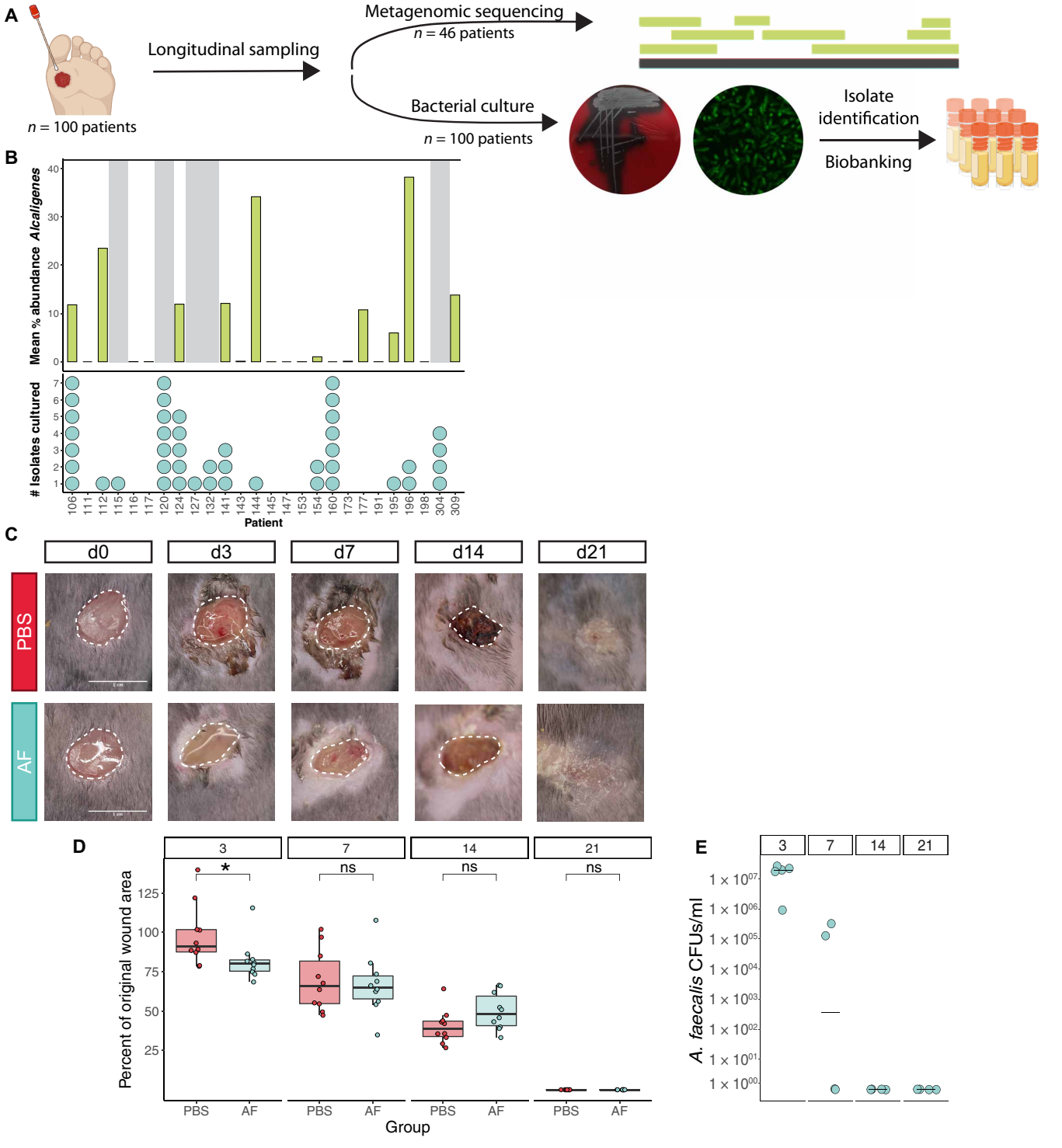

Fig. 1. *A. faecalis* is prevalent in the wound microbiome and promotes early diabetic wound healing. (**A**) Longitudinal samples collected from DFUs of 100 patients were cultured, and a subset of samples was sent for shotgun metagenomic sequencing. Representative images of *A. faecalis* streaked on blood agar and bacterial fluorescence in situ hybridization are shown. (**B**) Prevalence and abundance of *Alcaligenes* across the DFU-100 patient cohort. Top plot shows the mean percent abundance of *Alcaligenes* out of total bacteria for each patient sample's metagenomic data. Patients that were culture-positive but did not have samples sent to metagenomic sequencing performed are grayed out. The number of *A. faecalis* isolates cultured from unique patient samples are displayed in the bottom plot. (**C** and **D**) Wounds (8 mm) were created in diabetic mice and colonized with vehicle control (PBS) or *A. faecalis* (AF). Longitudinal wound images were taken at days 0, 3, 7, 14, and 21, and wound size (white dashed outline) compared to original wound area was quantified, demonstrating a significant decrease in AF-treated wound size at day 3. Scale bars, 1 cm; $n = 5$ mice per group and 2 wounds per mouse; $^*P < 0.05$, $P = 0.015$ by Wilcoxon rank sum test; data representative of two independent experiments. ns, not significant. (**E**) Wound tissue was harvested at each time point for *A. faecalis* CFU quantification. $n = 4$ mice per group (day 3 = 5 mice) and 1 wound per mouse.

Table 1. *Alcaligenes* is frequently identified in several chronic wound types. Studies of several chronic wound types including DFUs, VLUs, and SCLUs have identified *Alcaligenes* as a prevalent and abundant component of the wound microbiome. Citations by wound type are shown, along with the method of *Alcaligenes* identification and whether species-level identification was resolved. Measures of abundance or prevalence are shown in the footnote.

	***A. faecalis* identified in chronic wounds**			
Wound type	**Cultured?**	**Sequenced?**	**Species-level ID?**	**Abundance or prevalence**
DFUs				
Citron *et al.* (*33*)	Y	N	Y	2.2*
Min *et al.* (*34*)	N	Y	N	3.4†
Jnana *et al.* (*35*)	N	Y	N	–
Mixed				
Dowd *et al.* (*36*)	N	Y	Y	1.06 (V), 0.10 (F), 0.07 (P)‡
Mahnic *et al.* (*37*)	Y	Y	Y	–
VLUs				
Thomsen *et al.* (*38*)	Y	Y	Y	–
Ernlund *et al.* (*39*)	N	Y	N	72*
SCLUs				
Byeon *et al.* (*40*)	N	Y	N	5†

*% of patient cohort with identified *Alcaligenes*. †Relative abundance. ‡% of total sequences.

A. faecalis treatment improved the overall epithelialization potential of keratinocytes, including migration and proliferation, in both human and mouse diabetic skin.

Given our findings that bacteria-free, sterile supernatant from *A. faecalis* conditioned media induces the prohealing response, we hypothesized that *A. faecalis* exerts its effect through release of a secreted molecule. To test this hypothesis and characterize the secreted factor, we performed size fractionation on conditioned media with 3- and 10-kDa filters (Fig. 2D). If the molecule is larger than the filter size, then the activity should only be found in the larger fraction. We found that the proepithelialization activity is concentrated in both the >3- and >10-kDa fractions, indicating that the active molecule is likely larger than 10 kDa. Bacterial secreted molecules of this size are often small peptides as "small molecules" such as metabolites are definitionally <1 kDa in size. To test if the active molecule is sensitive to protease treatment, we performed the scratch closure assay with proteinase K-treated *A. faecalis* conditioned media. Consistent with our hypothesis, protease treatment abrogated the activity of the conditioned media (Fig. 2D). Thus, *A. faecalis* can induce a proepithelialization phenotype likely through secretion of a small peptide.

MMP expression in diabetic wounds is down-regulated by *A. faecalis* treatment

Because *A. faecalis* promoted epithelialization processes in diabetic skin, we next investigated the potential mechanisms. To determine how *A. faecalis* treatment influences transcriptional programs in diabetic wounds, we treated murine diabetic wounds with *A. faecalis* as described for Fig. 1B and subsequently harvested wounds after 3 days for RNA extraction and RNA sequencing (RNA-seq) (Fig. 3A). These wounds were compared to PBS-treated wounds as a negative vehicle control and *S. aureus*–treated wounds to represent a pathogen-mediated wound healing response.

Treatment with *A. faecalis* induced a distinct transcriptional profile in day 3 wounds compared to vehicle control or *S. aureus* (Fig. 3B). We performed unsupervised hierarchical clustering of differentially expressed genes (DEGs) of the *A. faecalis*–treated and vehicle-treated groups, demonstrating the modules of up- and down-regulated genes that are distinct in each group (Fig. 3C). Treatment with *A. faecalis* led to a greater number of significantly down-regulated genes versus up-regulated (119 versus 74, respectively). These results are in contrast to the response of pathogenic *S. aureus* treatment, which resulted in increased expression of many more genes (440) (fig. S3A).

A. faecalis significantly up-regulated *Colq*, encoding for a subunit of acetylcholinesterase, as well as the immune-related genes *Cd4* and *Vcam1* (Fig. 3D). Accordingly, gene ontology (GO) analysis demonstrates that the significantly up-regulated gene signatures are related to leukocyte recruitment and T cell activation (Fig. 3E). We performed a broad-based survey of the immune response to *A. faecalis* by performing flow cytometry on *A. faecalis*–treated and vehicle-treated wounded diabetic skin (fig. S3E). Total T cell receptor β–positive ($TCR\beta^+$) T cells, macrophage, and monocyte counts were similar between the two groups. However, there was a trend of increased $CD4^+$ T cell and neutrophil recruitment with *A. faecalis* treatment compared to vehicle control, consistent with the up-regulated GO pathways.

Of the genes that were down-regulated by *A. faecalis*, the most significant were those related to MMPs, notably *Mmp10* and its substrates *Lamc2* and *Lama3* (*50*, *51*). The down-regulated GO pathways were accordingly enriched for signatures related to MMP activity, such as collagen degradation and peptidase activity. In contrast, *S. aureus* treatment led to an enrichment in GO terms related to peptidase activity, including the gene member *Mmp10* (fig. S3, B and C). *S. aureus* also induced a much stronger signature of immune responses to pathogens, with significantly enriched GO terms for cell death, defense responses, and interferon-γ (IFN-γ) signatures (fig. S3C); none of these GO pathways were significantly up-regulated by *A. faecalis*. Individual genes that map to these pathways are shown in fig. S3D. Shown are multiple genes related to IFN and tumor necrosis factor signaling as well as neutrophil recruitment that are up-regulated by *S. aureus* treatment but are unchanged or decrease with *A. faecalis* treatment.

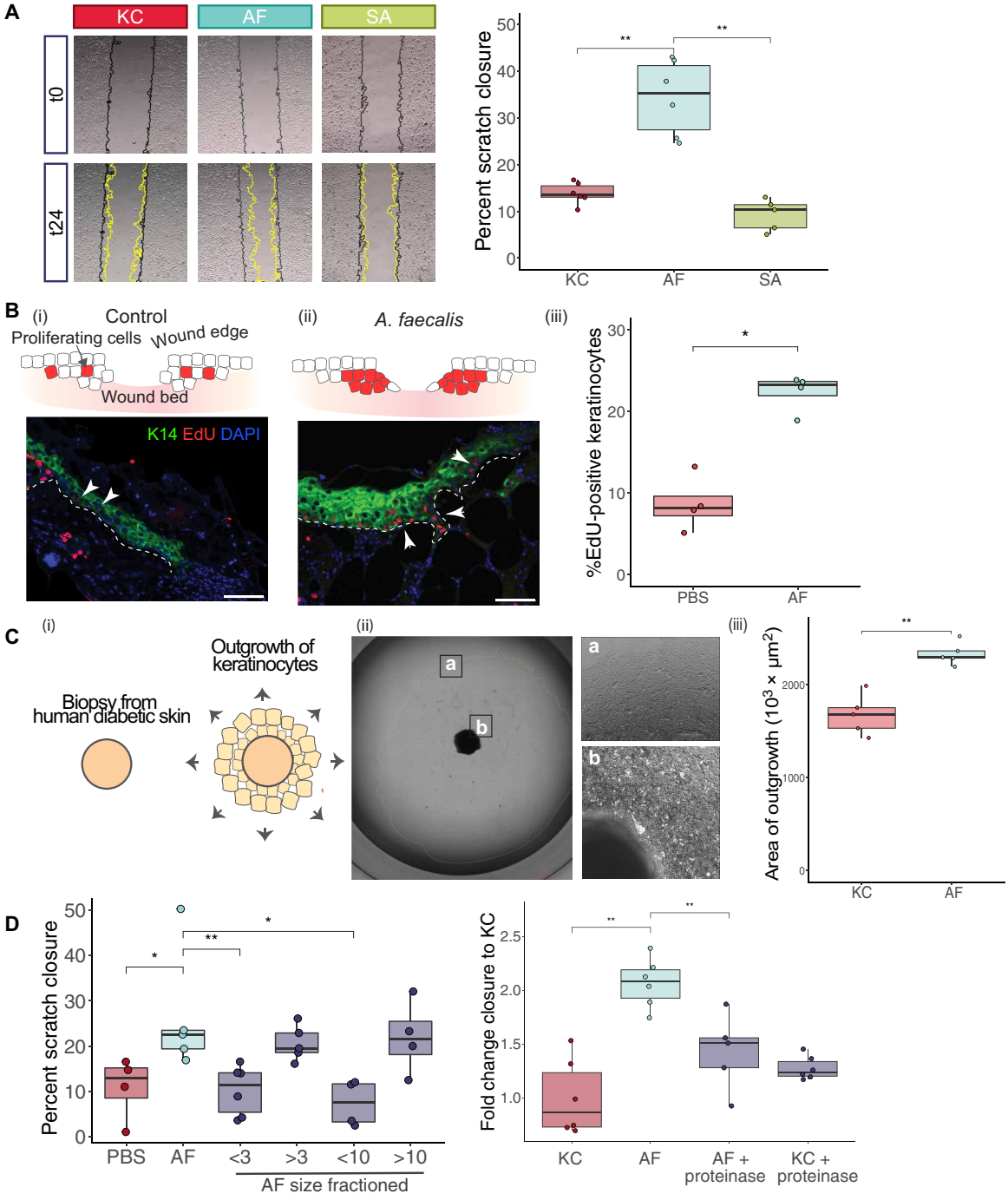

Fig. 2. *A. faecalis* enhances diabetic keratinocyte migration and proliferation. (**A**) Gaps were created in diabetic mouse keratinocytes and treated with conditioned media, and in vitro wound closure was measured at 24 hours. Cells were treated with vehicle control [keratinocytes (KC)], 10% *A. faecalis* conditioned media (AF), or 10% *S. aureus* conditioned media (SA). Initial gap size is drawn in black, and migrating margins are drawn in yellow. Data representative of >3 independent experiments; $n = 6$ gaps per group. (**B**) Wounds (8 mm) were created in diabetic mice and colonized with PBS (i) or AF (ii). At 3 days after wounding, mice were injected with EdU to label proliferating cells. Wound tissue was stained for EdU-positive cells (white arrows), and epithelial cells were identified by K14. Wound edges were imaged ($n = 4$ wounds per condition), and % EdU^+ $K14^+$ epithelial cells was determined [number of EdU^+ $K14^+$ cells (red nuclei)/total $K14^+$ cells (green cells)] (iii). [In panels (i) and (ii), white dashed lines are the dermal-epidermal junctions; scale bars (bottom right), 100 µm.] (**C**) Ex vivo explant outgrowth assay to measure the epithelialization potential of human diabetic keratinocytes. (i) Biopsies (1.5 mm) are taken from human diabetic skin, and keratinocyte growth from the explant is quantified. (ii) Representative bright-field image of the explant edge (b) and border of the keratinocyte outgrowth (a) after 10 days of incubation. (iii) Explants were incubated with AF or KC, and keratinocyte outgrowth area was quantified at day 10; $n = 5$. (**D**) Scratch closure assay performed as described in Fig. 2B. Left graph shows results of AF size-fractioned conditioned media with 3- and 10-kDa filters. Right graph shows results from proteinase K-treated AF and KC conditions, quantified as fold change to KC treatment alone. For all plots: $*P \leq 0.05$; $**P \leq 0.01$ by Wilcoxon test.

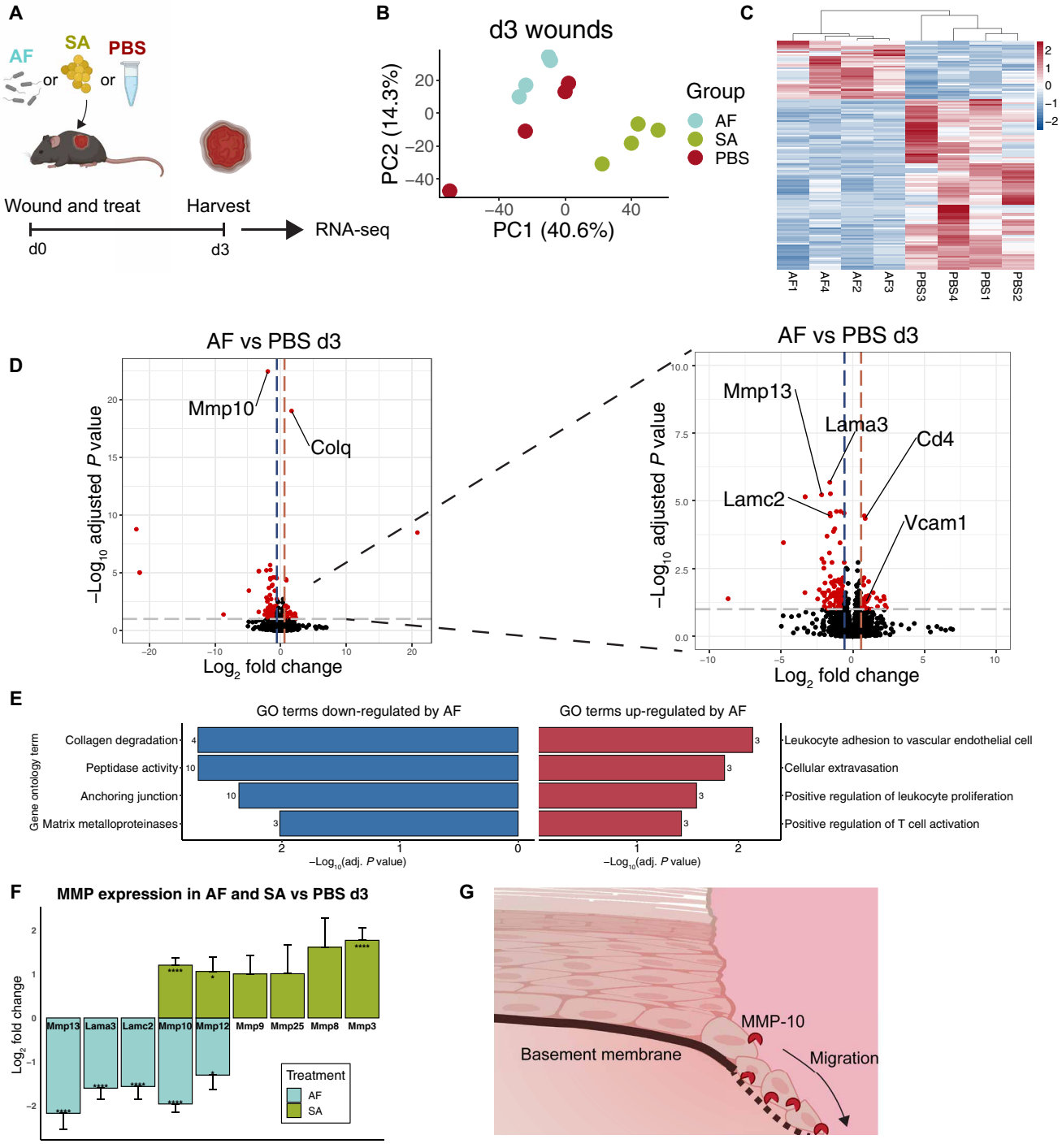

Fig. 3. *A. faecalis* treatment decreases MMP expression in murine diabetic wounds. (**A**) Experimental overview for RNA-seq performed on diabetic murine wounds treated with *A. faecalis* (AF), *S. aureus* (SA), or vehicle control (PBS); $n = 4$ mice per group and 1 wound per mouse. (**B**) Principal components analysis on day 3 wounds demonstrates distinct clustering of the three treatment groups. (**C**) Heatmap of DEGs (with FDR < 0.01) between the AF and PBS groups at day 3. Unsupervised clustering using Spearman's correlation was used for hierarchical clustering of the samples, while Pearson's correlation was used for gene clustering (heatmap rows; dendrogram not shown). Colors are used to codify log fold change values, with red values for increased expression and blue values for decreased expression. (**D**) Volcano plot demonstrating DEGs in AF versus PBS wounds at day 3. Horizontal dashed line represents a cutoff for the FDR *P*-adjusted value of <0.1. Vertical lines denote a fold change of ±1.5-fold. Genes that surpass both the *P* value and fold change cutoff are marked in red, with genes that are down-regulated by AF to the left of the plot and up-regulated to the right. The inset shows the same volcano plot but at a higher resolution. Significant genes of interest are highlighted with gene names on the plot. (**E**) GO enrichment was performed on DEGs for AF versus PBS at day 3. Up- and down-regulated GO terms of interest are highlighted, with the number of genes matching the term adjacent to the bar plot. (**F**) Gene expression changes of MMPs and related genes in AF versus PBS and SA versus PBS day 3 wounds; **P* adjusted < 0.05; *****P* adjusted < 0.5×10^{-4}. (**G**) Conceptual model demonstrating the activity of MMP-10 at the epidermal wound tongue.

Of particular interest is the inverse pattern of MMP-related gene expression. Unlike the significant down-regulation of several MMPs induced by *A. faecalis*, *S. aureus* induces increased expression of six different MMP encoding genes, with MMP-10 being the most significantly different between the two groups (Fig. 3F; *P adjusted < 0.05; ****P adjusted $< 0.5 \times 10^{-4}$). During wound healing, MMP-10 is expressed by keratinocytes at the leading edge of the wound and degrades the extracellular matrix (ECM) components that provide a substrate for keratinocyte migration (Fig. 3G) (*50*, *52*, *53*). However, excessive expression of MMPs, which is promoted by diabetes and hyperglycemia, is deleterious to healing (*28*, *54*–*56*). Together, our results suggest that *A. faecalis* promotes diabetic wound healing by inhibiting MMP expression locally to promote reepithelialization.

Reduction of excess MMP-10 mediates the proepithelialization effects of *A. faecalis*

We focused on MMP-10 as a potential mechanism because it was the most significantly DEG and is expressed by keratinocytes at the wound leading edge. To begin to test the hypothesis that *A. faecalis* is moderating MMP-10 levels to promote reepithelialization, we correlated the RNA-seq results with protein expression during diabetic wound healing. We performed immunofluorescence staining for MMP-10 on day 3 wounds (Fig. 4A). Consistent with previously reported expression patterns (*52*, *53*, *57*), MMP-10 was more highly expressed in wound tongue, nearest the wound bed, compared to sparse epidermal staining in sites distal from the wound bed. MMP-10 protein levels in the proximal wound epidermis trended toward reduction in *A. faecalis*–treated wounds compared to vehicle control (Fig. 4B; $P = 0.081$ by Wilcoxon rank sum test; sample ImageJ analysis shown in fig. S4A and no primary antibody control in fig. S4B).

Although we have focused on the epidermal keratinocyte contribution of MMP-10, macrophages can be another source of MMP-10 in the dermal compartment of the skin. Therefore, we performed immunofluorescence staining of MMP-10 and the macrophage marker F4/80 to determine potential costaining of these two markers (fig. S4C). As seen in the negative control with no primary antibody, there is autofluorescent, nonspecific signal in the dermis. Much of the "true-positive" MMP-10 signal is found in the epidermis (red arrows). Macrophages are sparse and scattered in the dermis (green arrows). Areas of true MMP10-F4/80 colocalization are highlighted with the red-green arrows. Much of the autofluorescent signal in the dermis is from red blood cells, a common source of autofluorescence (*58*), as stained by the antibody TER-119 in fig. S4C.

Next, we tested the dependence on MMP-10 reduction for the pro-healing effects of *A. faecalis* treatment by performing a scratch assay with murine diabetic keratinocytes as described in Fig. 2A. The keratinocytes are seeded on a thin coating of Matrigel, a basement membrane substrate made up of ECM proteins that are digested by MMP-10. To mimic the overexpression of MMP-10 that can occur in diabetic wounds, exogenous recombinant mouse MMP-10 (rMMP-10) was added to *A. faecalis* conditioned media. Addition of excess rMMP-10 significantly abrogates keratinocyte migration observed with *A. faecalis* conditioned media alone (Fig. 4C; **$P < 0.01$ by Wilcoxon rank sum test). These differences are not due to changes in keratinocyte viability after 24-hour incubation with the bacterial conditioned media (fig. S2B).

For in vivo validation of these findings, we compared *db*/*db* wound sizes of *A. faecalis*–treated wounds with those treated with *A. faecalis* plus rMMP-10. As previously observed, *A. faecalis* leads to significantly decreased wound sizes compared to vehicle control at day 3 (Fig. 4D; *$P \leq 0.05$; **$P \leq 0.01$ by Wilcoxon rank sum test). However, addition of excess rMMP-10 leads to significantly larger wounds than *A. faecalis* alone, leading to wound sizes that are similar to the vehicle-treated control group. Wounds treated with *A. faecalis* and rMMP-10 retained high levels of *A. faecalis* colonization (fig. S5A). Although there was a decrease in *A. faecalis* CFU counts compared to *A. faecalis* alone, this slight decrease is likely due to increased wound size allowing for colonization of other bacterial species, as seen by wound CFU plating. Wounds treated with rMMP-10 alone have similar defects in healing to vehicle control (fig. S5B). In addition to measuring MMP-10 RNA and protein levels by RNA-seq and immunofluorescence, we also measured MMP-10 activity in vehicle- and *A. faecalis*–treated day 3 wound tissue (fig. S5C). Consistent with the RNA and protein results, we observe decreased MMP-10 activity with *A. faecalis* treatment, although the differences were not statistically significant.

Wound area results were consistent with epidermal tongue quantification. We used immunohistochemical elastin staining to facilitate epithelialization quantification (Fig. 4E). Elastin in the dermis is a good marker of the original wound edge as it is not present in the day 3 wound bed. Therefore, we quantified the length of the epidermal tongue relative to the original wound edge, as previously described by Linehan *et al.* (*18*). We found that *A. faecalis*–treated wounds were initiating reepithelialization, as evidenced by visible wound tongues. However, the vehicle- and rMMP-10–treated groups had little keratinocyte migration at the wound edge. We even observed "negative" tongue lengths in these groups, where there was keratinocyte cell death at the edge of the wound. These results are reflected by the >100% original wound area observed in these groups at day 3 (as in Fig. 4D). To further examine how excess MMP-10 expression affects wound edge morphology, we also performed immunohistochemistry on the wound samples, using Masson's trichrome stain to distinguish the epidermal tongue from the underlying dermis (fig. S5D). We similarly observe wound tongue formation in the *A. faecalis*–treated group, but addition of excess MMP-10 disrupts this initiation of reepithelialization. Together, these results indicate that *A. faecalis* promotes early diabetic wound closure by decreasing rMMP-10 overexpression (Fig. 4F).

DISCUSSION

Improved therapeutic approaches are needed for nonhealing wounds as they present a major challenge to the health care system by increasing treatment costs as well as rates of morbidity and mortality. The skin microbiome exists at the interface of all cutaneous wounds, but its potential as a therapeutic target remains relatively untapped. We previously deeply characterized the microbiome of DFUs by shotgun metagenomic sequencing and culture-based approaches. In addition to wound pathogens and skin-resident commensals, we also detected microbes that have not been studied in the context of wound healing. Here, we focused on determining the functional relevance of what was previously considered a wound "bystander" or contaminant, *A. faecalis*. Our findings show that *A. faecalis* treatment promotes diabetic wound closure by enhancing the epithelialization potential of diabetic keratinocytes. *A. faecalis* treatment of diabetic wounds down-regulated expression of MMPs, which are overexpressed in diabetic skin and contribute to delayed wound repair. Thus, our results suggest that leveraging selective interactions between microbiota and host could target specific process that are dysregulated during diabetic wound healing.

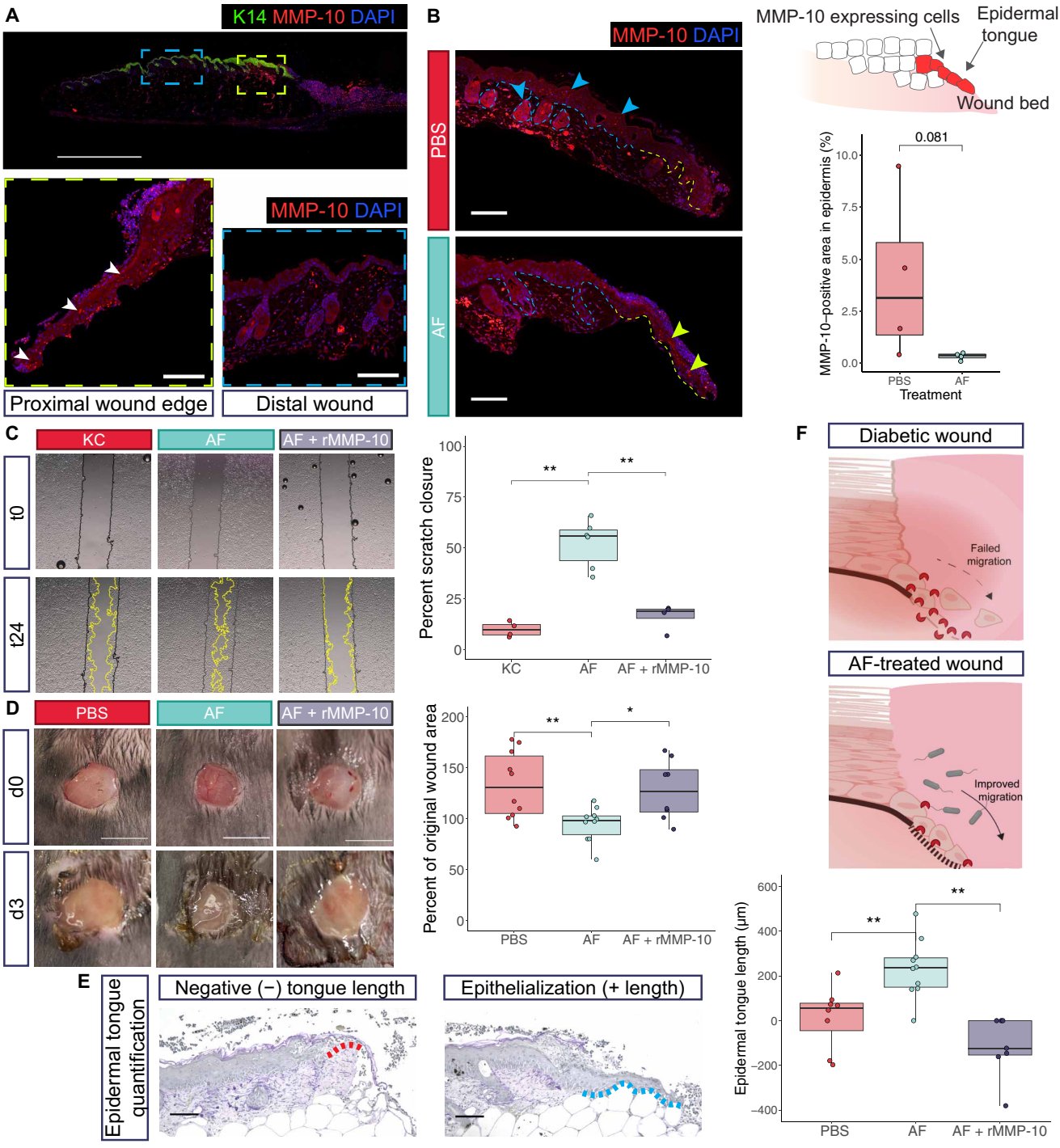

Fig. 4. The prohealing phenotype of *A. faecalis* is dependent on MMP-10 reduction. (**A**) Immunofluorescence staining was performed on day 3 wound tongues. Keratin 14 (K14), MMP-10, and nuclear (DAPI) costaining were performed. Scale bar, 1000 μm. Blue and green boxes indicate locations of higher-magnification insets. The positive MMP-10 signal is highlighted by white arrowheads in the proximal wound edge, while there is negative MMP-10 staining in the distal wound epidermis. Scale bars, 100 μm. (**B**) The percentage of epidermal area with a positive MMP-10 signal was calculated in the epidermis adjacent to the wound bed. The green dashed line highlights the proximal wound tongue, while the blue dashed line is distal wound epithelium. Arrowheads highlight areas of MMP-10–positive signal. Scale bars, 250 μm, $n = 4$ mice per group; $P = 0.081$ by Wilcoxon rank sum test. (**C**) Gaps were created in diabetic mouse keratinocytes, and in vitro wound closure was measured at 24 hours. Initial gap size is drawn in black, and migrating margins are drawn in yellow. rMMP-10, 200 ng/ml murine recombinant MMP-10 added to AF [$n = 5$ gaps per group (except $n = 6$ for AF condition); data are representative of >3 independent experiments]. (**D**) Wounds (8 mm) were created in diabetic mice and colonized with PBS, AF, or AF + rMMP-10. Wound images were taken at days 0 and 3, and wound size compared to original wound area was quantified. Scale bars, 1 cm; $n = 5$ mice per group (4 per group for AF + rMMP-10) and 2 wounds per mouse. (**E**) Quantification of epidermal tongue length was performed on wound sections from (D). Representative elastin stains are shown. For all plots: $^*P \leq 0.05$; $^{**}P \leq 0.01$ by Wilcoxon rank sum test. (**F**) Conceptual model of improved migration with AF-mediated decreased MMP-10 expression.

A. faecalis has been previously characterized as an environmental bacterium found in water and soil and rarely causes infection (*25*, *59*). The consistent detection of *A. faecalis* through both culture- and sequencing-based methods, with some patients being colonized across multiple time points, indicates that *A. faecalis* is likely a wound inhabitant rather than transient contaminant. In line with this hypothesis, *A. faecalis* has been detected in multiple wound types across the globe (*33*–*40*). It has been referred to as a member of the "core microbiome" in DFUs (*35*) and noted as an abundant, understudied bacteria "that should be considered in future studies" (*34*). Here, we show that *A. faecalis* could play a more substantial role in wound healing by enhancing reepithelialization and inhibiting aberrant expression of proteases that are detrimental to wound healing. These results demonstrate the importance of looking beyond wound pathogens in the pursuit of actionable therapeutic targets in the wound microbiome.

It is well established that MMPs are dysregulated in diabetic healing (*26*), whereby MMPs are overexpressed and overactivated, along with a concomitant decrease in their inhibitors (*27*–*29*). This imbalance has been shown to inhibit proper keratinocyte migration and delay healing (*30*–*32*). We focused specifically on MMP-10 or stromelysin 2 as it was the most significantly decreased gene in the setting of *A. faecalis* treatment and was up-regulated by the pathogen *S. aureus*. In addition to transcriptional and protein detection of MMP-10 by immunofluorescence, we also assay MMP-10 activity directly through digestion of its substrate and indirectly by measuring early reepithelialization. In our ex vivo measurement of MMP-10 activity, the observed lack of statistical difference could likely be due to shortcomings of the assay including use of human MMP-10 substrate (no mouse substrate is available for such an assay) and that other MMPs present in the tissue may degrade the substrate. Under normal healing conditions, MMP-10 facilitates reepithelialization by cleaving hemidesmosome and desmosome components to release keratinocytes from both the ECM and cell-to-cell adhesions, respectively (*51*). It is typically only expressed in wounded keratinocytes and exclusively localized to the migrating tip of the epidermal tongue (*52*, *53*, *57*). Furthermore, this peptidase has been shown to be increased diabetic skin (*53*) and other diabetic epithelium (*60*). Increased expression of MMP-10 has been shown to inhibit reepithelialization (*57*). Constitutive overexpression of MMP-10 leads to an abnormal migrating epidermal tip with "scattered" keratinocytes, inappropriate keratinocyte contact with ECM components, and apoptotic keratinocytes in the wound tongue (*50*).

Although our studies focus on the effects of MMP-10 in the wounded epidermis, it is possible that MMP-10 overexpression may be affecting other wound healing compartments. For example, MMP-10 has been shown to regulate resident macrophage collagenase activity in the skin (*61*). Our immunofluorescence staining of MMP-10 and macrophages demonstrates occasional colocalization of MMP-10 and F4/80 signal near the wound bed. However, a higher density of true-positive MMP-10 signal is found in the epidermis. Given the importance of temporal, spatial, and cellular dynamics for MMP signaling, future investigations will take advantage of high-resolution methods to parse apart these dynamics.

MMP activity, like any inflammatory process, needs to be finely tuned and balanced during healing (*62*), including a well-orchestrated temporal and spatial localization of MMP expression (*63*, *64*). This organization is disrupted in diabetic wounds, which are considered "stuck" in the early inflammatory phase, and unable to progress to the proliferative phase (*26*). We observe that *A. faecalis* exerts its strongest benefit in these crucial few days of wound healing during this transition from the inflammatory stage to reepithelialization. During this transition, keratinocytes must begin to both proliferate and migrate to the wound site. Keratinocyte migration is suspected to be the rate-limiting step in nonhealing wounds (*65*) and therefore a critical target for wound healing therapies. Therefore, by rebalancing MMP-10 expression, *A. faecalis* may be able to push diabetic wounds toward a proepithelialization environment. This work may also have implications beyond DFUs as MMPs are up-regulated in PUs and VLUs (*66*, *67*), which are also commonly colonized by *A. faecalis* (Table 1).

Our in vitro work suggests that *A. faecalis* exerts its proepithelialization effect through secretion of a small peptide. This microbial mechanism is particularly exciting because bacterial-derived molecules are well known to modulate host biology and are attractive sources of previously unidentified therapeutics. Although there has been recent works on the therapeutic potential of skin commensal-derived molecules, most studies have focused on antimicrobials (*68*–*72*), whereas bacterial molecules that promote wound healing responses are yet to be uncovered. Future work will be needed to delineate the pathway by which a secreted peptide from *A. faecalis* modulates keratinocyte MMP expression to promote epithelialization. Keratinocytes are the first responders of the innate immune system to skin barrier breach. As such, they are equipped with myriad receptors that detect bacterial products. There is growing appreciation for injury signals, beyond pathogen- and damage-associated molecular patterns (*73*), that are detected by keratinocytes and can induce reepithelialization (*74*). It is reasonable to hypothesize that an *A. faecalis*–derived peptide is sensed by keratinocyte receptors and induces a promigratory phenotype, although the identity of that signal will need to be identified in future studies.

We did not find any correlative evidence from human studies to suggest that *A. faecalis* influences clinical outcomes of wound healing. This could be due to insufficiently powered studies or, alternatively, biological factors that limit the effect of a single microbe in a greater network of microbe-microbe and host-microbe interactions. For example, other members of the wound microbiome may limit the growth and effect of *A. faecalis*, either through direct inhibitory mechanisms or by nutrient limitation. Furthermore, the presence of pathogens in the same microbiome may induce greater tissue damage than is able to be overcome by the positive effects of *A. faecalis*. However, our reductionist approach was valuable in delineating the functional potential of *A. faecalis*. Expanding these findings to a community-wide framework will be crucial to understanding how prohealing "commensals" interact with pathogens and other members of the wound microbiome. These interactions will need to be considered for the success of any microbial-directed therapy for wound healing.

Our goal was to investigate the "dark matter" of the wound microbiome and resulted in identification of *A. faecalis* as a wound resident with the potential to correct aberrant processes that lead to delayed healing. These results reveal a previously unidentified therapeutic target and underscore why the wound microbiome, beyond well-established pathogens, should be considered. In light of broad-spectrum antibiotic therapies that deplete commensal microbes such as *A. faecalis* while selecting for pathogen resistance and virulence, our work underscores the need for judicial antibiotic prescription for chronic wounds, especially in the absence of clinical signs of infection (*75*). Further dissection of these complex host-microbiome dynamics during tissue

repair of *A. faecalis* and other members of the wound microbiota should reveal additional promising therapeutic targets for chronic wounds.

MATERIALS AND METHODS

Culture- and sequencing-based detection of *A. faecalis* in DFUs

Longitudinal samples for microbial analysis were collected from DFUs of 100 patients as previously described (*76*, *77*). Swabs were collected using the Levine technique to sample deep tissue fluid (*78*), resuspended in tryptic soy broth (TSB), and plated on blood agar, eosin-methylene blue agar, and Chromagar plates. *A. faecalis* isolates were identified from eosin-methylene blue agar plates by morphology and Gram staining for Gram-negative rods, using standard microbiological procedures (*79*). The isolates were further identified by Sanger sequencing of the 16*S* ribosomal RNA gene and matrix-assisted laser desorption/ionization–time-of-flight mass spectrometry at the Pennsylvania Animal Diagnostic Laboratory System. Metagenomic sequencing was performed on a subset of the DFU specimens as previously described (*24*). *Alcaligenes* abundance was estimated using MetaPhlAn2 with default parameters and is reported as the mean % of bacterial abundance across samples from each patient (*80*).

Bacterial strains and preparation

The *A. faecalis* (EGM#4-61) and *S. aureus* (EGM#5-76) strains were cultured as described above and maintained in the Grice Lab culture repository (number in parenthesis indicates unique laboratory identifier code). Bacteria were prepared for wounding treatment by streaking onto blood agar and incubating at 37°C for 24 hours. Single colonies were then used to inoculate TSB and then grown by shaking at 250 rpm at 37°C for 18 hours. The bacteria culture was then spun down at 13,000 rpm for 2 min. To prepare a glycerol stock, the pellet was resuspended in PBS with 10% glycerol then kept at −80°C until the day of wounding. At the same time, a portion of the overnight culture was serially diluted and plated for CFU calculation.

Bacterial conditioned media preparation and biochemical characterization

For conditioned media preparation, the strains were streaked out on blood agar and grown in TSB as described above. The TSB bacterial culture was then used to inoculate human keratinocyte media without antibiotics and grown by shaking at 250 rpm at 37°C for 24 hours. The bacteria culture was then spun down at 4000 rpm for 30 min at 4°C. The supernatant was passed through a 0.22-μm filter for sterilization. At the same time, a portion of the overnight culture was serially diluted and plated for CFU calculation.

For size fractionation, the conditioned media was prepared as above. Then, 5 ml of conditioned media was spun down using the Amicon Ultra-15 Centrifugal Filter Devices 3000- and 10,000–molecular weight cutoffs at 5000*g* for 40 min at 4°C. The two fractions were brought to the same volume to account for concentrating effects of the filters using keratinocyte media and then added to cells for the scratch closure assay as described below. For protease treatment of conditioned media, thermolabile proteinase K was used for digestion. Proteinase K (NEB) was diluted 1:50 and added to conditioned media, incubated for 1 hour at 37°C, then heat-inactivated for 10 min at 55°C for subsequent cell treatment.

Animal models and husbandry conditions

All mouse experiments were conducted under protocols approved by the University of Pennsylvania Institutional Animal Care and Use Committee (protocol no. 804065). All mice were housed and maintained in an ABSL II and specific pathogen–free facility in the Clinical Research Building vivarium at the University of Pennsylvania. The following strain of mice was used in these studies: B6.BKS(D)-*Lepr*$^{db/db}$/J (JAX stock no. 000697) (*41*).

Excisional wounding and bacterial colonization of murine diabetic wounds

One day prior to wounding, the mouse dorsum was shaved with an electric razor. Mice were singly housed on the day of wounding. Pain control was administered with extended-release buprenorphine and bupivacaine injections, and isoflurane was administered for anesthesia. Two full-thickness excisional wounds were made on each mouse back using an 8-mm punch biopsy tool (Miltex). For bacterial treatment of wounds, 2×10^8 CFU of *A. faecalis* or *S. aureus* in 10 μl of PBS was applied to each wound. For vehicle control treatment, the same volume of PBS with 10% glycerol was applied to the wounds. All wounds were photographed and measured at time of wounding (day 0) and subsequent time points (e.g., day 3). After day 0 imaging, the wounds were covered with Tegaderm (3M) to prevent external bacterial contamination. Tegaderm was left on until day 3 wound imaging, and if the experimental timeline continued, wounds were re-covered with Tegaderm until day 7. Wounds were blinded and then quantified in ImageJ (version 1.53k) using a ruler-calibrated measurement, with each wound being measured three independent times.

For addition of exogenous MMP-10 to the wounds, murine recombinant MMP-10 (RayBiotech, 230-00748-10) was diluted in PBS and 4 μg was added to each wound. This dose was scaled to a similar molarity as previous rMMP treatments of wounds (*81*). For protein and vehicle control, purified bovine serum albumin (Sigma-Aldrich) was diluted in PBS to the same molarity as rMMP-10 and then added to the PBS control and *A. faecalis* treatment.

Bacterial CFU quantification of wounds

For bacterial quantification from wound tissue, a 12-mm punch biopsy tool (Miltex) was used to dissect the wound bed and surrounding wound edge tissue from the back skin. Wound tissue was homogenized with horizontal vortexing using ceramic beads (MP). The homogenate was serially diluted, and each dilution was plated in duplicate on blood agar plates to quantify CFUs. For bacterial quantification by swabbing, sterile cotton tipped applicators (Puritan) were dipped in PBS and used to swab the wound bed using the Levine technique (*78*). Swabs were collected in PBS, and the PBS was subsequently serially diluted and plated on blood agar as described above.

Murine diabetic keratinocyte derivation

Primary keratinocytes were derived from tail skin of adult *db/db* diabetic mice [B6.BKS(D)-*Lepr*$^{db/db}$] mice as previously described (*82*). Briefly, skin was dissected from the tail bone and incubated in dispase (4 U/ml; Sigma-Aldrich) overnight at 4°C. The epidermis was then separated from the dermis, and the epidermis was incubated with 0.05% trypsin-EDTA at room temperature for 20 min. The digestion reaction was then quenched with Dulbecco's modified Eagle's medium (DMEM) + 5% fetal bovine serum (FBS). A single-cell suspension was generated by vigorously rubbing the epidermal sheet against a petri dish. The cell suspension was then passed through

a 100-μm filter and centrifuged at 4°C for 5 min at 180*g*. For plating, the cell pellet was resuspended in cold low Ca^{2+} keratinocyte serum-free media (Life Technologies) supplemented with bovine pituitary extract, human epidermal growth factor, 1% FBS, 4% DMEM, and antibiotics-antimycotics.

Scratch closure assay

Before keratinocyte seeding, cell culture plates were thin-coated with Matrigel (Corning), an ECM equivalent. Two-well inserts that create a defined cell-free gap (Ibidi) were placed in a 24-well plate. Primary diabetic keratinocytes (derivation described above) were seeded in the inserts at a density to reach 100% confluence the following day. After overnight incubation, the inserts were removed, cells were washed and then treated with 10% bacterial conditioned media or vehicle control (10% keratinocyte media used for bacterial growth). The starting wound gap was immediately imaged on the Keyence BZ-X710 (t = 0 hours). After 24 hour incubation at 37°C and 5% CO_2, the identical gap location was imaged (t = 24 hours). Microscope images were blinded, and gap area at t = 0 and t = 24 was quantified using the ImageJ "Wound healing size tool, updated" (*83*). For addition of exogenous MMP-10 to the scratches, murine recombinant MMP-10 (RayBiotech, 230-00748-10) was diluted in keratinocyte media to the indicated concentrations.

Viability of keratinocytes

The alamarBlue reagent (Invitrogen) was used to determine viability of primary diabetic keratinocytes. At the experimental endpoint, alamarBlue was diluted 1:10 in keratinocyte media and incubated for 4 to 6 hours, and the supernatant fluorescence was read with excitation at 560 nm and emission at 600 nm. Fluorescence of alamarBlue added to keratinocyte media alone was subtracted as background.

EdU incorporation, detection, and visualization

A protocol to detect proliferating cells in wounds was used to measure incorporation of modified thymidine analog EdU (*84*). Mice were injected with EdU (Abcam, no. ab146186) at 25 μg/g weight of mice 1 hour prior to euthanasia. Tissue was collected and fixed in 4% paraformaldehyde and paraffin-embedded and sectioned as described in subsequent sections. Tissue was deparaffinized (two times in Xylene Substitute, Sigma-Aldrich, catalog no. A5597), hydrated after a series of ethanol graded rinses (one time each in 100% ethanol, 95% ethanol, 70% ethanol, and 50% ethanol), and finally rinsed three times in 1X PBS. Tissue was permeabilized in 1X PBS containing 0.5% Triton X-100 for 1 hour and incubated in EdU detection cocktail. The EdU cocktail is made freshly each time and consists of the following: 100 mM tris-buffered saline (pH = 7.6), 4 mM copper sulfate, 100 mM sodium ascorbate, and 5 μM sulfocyanine azide (Lumiprobe Corporation, catalog no. B1330). Tissue was rinsed three times in 1X PBS and then incubated with 1:5000 dilution rabbit polyclonal anti–keratin 14 antibody (BioLegend, clone Poly19053) for 1 hour and then detected with 1:10000 dilution goat anti-rabbit IgG secondary antibody conjugated with Alexa Fluor 488 (Thermo Fisher Scientific, catalog no. A-11008). Tissue was counterstained with DAPI, cover-slipped, and imaged. Wide-field fluorescence images were acquired using a 20X lens objective on a Leica DM6000 wide-field fluorescence microscope at the University of Pennsylvania, School of Veterinary Medicine Imaging Core. Total EdU-positive epithelial cells (Krt14-positive cells that were also EdU-positive) were counted manually on the composite merged images using ImageJ cell counter feature.

Outgrowth assay

The explant keratinocyte outgrowth assay was modified as described previously (*49*, *85*). Diabetic skin discarded from Mohs surgery was obtained, and subcutaneous fat was removed with a scalpel. Explants were excised using a 1.5-mm dermal biopsy punch tool (Miltex) and adhered to the bottom of a 48-well tissue culture dish coated with collagen. The explants were secured using 2 μl of Matrigel and submerged in growth medium consisting of keratinocyte serum-free media with keratinocyte growth supplements (Life Technologies, no. 17005042) and Medium 154 (Life Technologies, no. M154500). Explants were treated with 10% *A. faecalis* conditioned media. Outgrowths from explants were imaged at 10 days after establishment on a Keyence BZ-X710 microscope (Plan Fluor 10X lens) equipped with a motorized stage. The images were stitched using the built-in algorithm accompanying the BZ-X wide image viewer, and area of outgrowth was measured using ImageJ.

RNA-seq of wound tissue

Sample preparation and sequencing

To harvest wounds for RNA-seq, a 12-mm punch biopsy tool (Miltex) was used to dissect the wound bed and surrounding wound edge tissue. Tissue was then immediately snap frozen on liquid nitrogen. For RNA extraction, tissue was first cryo-pulverized using the CP02 CryoPrep automated dry pulverizer (Covaris). TRIzol (Invitrogen)–based phenol-chloroform extraction was then performed for RNA purification, followed by on-column DNase digestion (Qiagen). RNA integrity was assessed with a 2100 Bioanalyzer and the Eukaryote Total RNA 6000 Pico Kit (Agilent). All but one sample had an RNA integrity number of >6. RNA concentration was quantified on Qubit using the RNA Broad Range assay (Invitrogen). Library preparation and sequencing were performed by the Children's Hospital of Philadelphia High Throughput Sequencing Core. Ribosomal RNA was depleted, and libraries were constructed using the Illumina Stranded Total RNA Prep with Ribo-Zero Plus (Illumina) using 100 ng of RNA input. IDT for Illumina UD indexes were ligated to the libraries. Library quality control was performed, and then libraries were sequenced on the NovaSeq 6000 using the S2 flow cell, generating 50–base pair paired-end reads.

Analysis

Quality control was performed on the sequencing reads using FastQC (version 0.12.1) (*86*). Reads were mapped to the reference genome [Genome Reference Consortium Mouse Build 39 (GRCm39)] using kallisto (version 0.48.0) (*87*). Subsequent analysis was performed in the R computing environment (version 4.1.3) in RStudio (version 2022.02.1+461). Transcript-level abundances were imported with tximport (version 1.22.0) using the length-scaled transcripts per million (*88*). Differential gene expression analysis was performed using the DESeq2 package (version 1.34.0) (*89*). Variance-stabilized data were used for principal components analysis. Pairwise DEGs between treatments were obtained by setting corresponding "contrasts" for each pairwise comparison. The Benjamini-Hochberg (B-H) procedure was used as a multiple-testing correction for adjusted *P* values (*90*). GO analysis was performed using the gprofiler2 package (version 0.2.1), and the B-H correction method was used to adjust the enrichment *P* values (*91*).

Immune survey of wounds

Wounds for flow cytometry analysis were created with a small punch biopsy tool of the diabetic mouse ear pinnae. Then, 2×10^8 *A. faecalis* CFU or vehicle control was added to each ear and spread with a swab. On day 3 after wounding, ears were harvested for flow cytometry, and colonization was confirmed by CFU plating.

For single-cell suspension preparation, dorsal and ventral sides were separated and finely minced in RPMI 1640 media (Thermo Fisher Scientific) complemented with 10% FBS (R&D Systems) (cRPMI) containing Liberase TL (100 μg/ml; Roche) and DNase I (50 μg/ml; Sigma-Aldrich). Minced tissue was incubated with shaking at 37°C for 1 hour and then strained through a 70-μm filter into a new tube containing 1 ml of cRPMI. Cells were stained with cell surface stains and live-dead stain at 4°C for 15 min in PBS. Flow cytometry was then performed using an LSR Fortessa instrument (BD Biosciences). Compensation was performed using compensation beads (BD Biosciences, 552845). Flow cytometry data were analyzed using FlowJo software (TreeStar). Staining antibodies used included the following: CD45.2 (mouse, BUV395 fluorochrome, clone 104, BD Biosciences 564616, 1:200 dilution), TCRβ (mouse, BV605 fluorochrome, clone H57-597, BioLegend 562840, 1:200 dilution), CD4 (mouse, BUV737 fluorochrome, clone RM4-5, BioLegend 612844, 1:200 dilution), CD8a (mouse, PerCP-Cy5.5 fluorochrome, clone 53-6.7, BioLegend 100734, 1:200 dilution), Ly6G (mouse, allophycocyanin fluorochrome, clone 1A8, BioLegend 560599, 1:200 dilution), CD11b (mouse, BV421 fluorochrome, clone M1/70, Invitrogen 404-0112-82, 1:80 dilution), MHCII [mouse, fluorescein isothiocyanate (FITC) fluorochrome, clone M5/114.15.2, Invitrogen 11-5321-82, 1:200 dilution], CD64 (mouse, PE-Cy7 fluorochrome, clone 10.1, BD 561191, 1:200 dilution), Ly6C (mouse, BV785 fluorochrome, clone HK1.4, BioLegend 128041, 1:200 dilution), and Live/Dead Near-IR (Thermo Fisher Scientific L10119, 1:1000 dilution). CountBright beads were used for counting cells and normalization (Thermo Fisher Scientific, C36950).

The following gating strategy was used after gating on live cells > single cells > $CD45^+$: for T cells, $TCR\beta^+$; CD4 T cells, $TCR\beta^+$ > $CD4+CD8^-$; CD8 T cells, $TCR\beta^+$ > $CD8+CD4^-$; neutrophils, $TCR\beta^-$ > $Ly6G+CD11b+MHCII^-$; macrophages, $TCR\beta^-$ > $CD64+CD11b^+$; monocytes, $TCR\beta^-$ > $Ly6C+Ly6G^-$.

MMP-10 immunofluorescence sample preparation, detection, and visualization

Murine wound tissue was collected, fixed overnight in 4% paraformaldehyde, then paraffin-embedded and sectioned by the Cutaneous Phenomics and Transcriptomics (CPAT) core of the Penn Skin Biology and Diseases Resource-based Center (SBDRC). Immunofluorescence staining was also performed by the CPAT core. Tissue sections were deparaffinized and rehydrated as described above. Heat-induced antigen retrieval was performed in 0.01 M citrate buffer (pH 6.0) and blocked in 10% normal goat serum. The following primary antibodies were used for immunofluorescence staining: K14 1(1:500; BioLegend, 906004), MMP-10 (2.0 μg/ml; Invitrogen, PA5-79677), MMP-10 (1:100; Abcam, 261733), F4/80 (1:50; Invitrogen, 14-4801-82), and FITC-conjugated TER-119 (1:200; Invitrogen 11-5921-82). Primary antibodies were incubated overnight at 4°C. The following secondary antibodies were used: Alexa Fluor 488 conjugated goat anti-chicken (1:500; Invitrogen, A-11039); Alexa Fluor 555 conjugated goat anti-rabbit (1:1000; Invitrogen, A-21428); Alexa Fluor 594 conjugated goat anti-rabbit (1:500; Invitrogen A-11037); Alexa Fluor 647 conjugated goat anti-rat (1:1000; Invitrogen, A-21247); Alexa Fluor 488 conjugated goat anti-mouse (1:2000; Invitrogen A-11001).

Fluorescence images were taken on the Leica DM6B-Z fluorescence microscope using the 20X lens objective. Tiled images were stitched together in the LAS-X software (version 3.7.6.25997) and then prepared for export using Fiji (version 2.9.0) and processed in Adobe Photoshop (version 24.1.1). MMP-10 signal quantification was performed in ImageJ (version 1.53k); all images were blinded, and global thresholding was performed to the same value cutoff on all images to distinguish positive versus negative MMP-10 signal. A length along the epidermis equal to 1000 μm from the tip of the epidermal wound tongue was measured, and the epidermis of this segment was selected using the freehand tool. The total area was measured, and then the area of positive signal above the threshold was measured to calculate positive MMP-10 signal in the epidermis.

Trichrome and elastin staining and visualization

Wound sections were prepared, embedded, and deparaffinized as described above. Masson's trichrome staining and Luna elastin staining were performed by the CPAT core of the SBDRC. Brightfield images were taken on the Keyence BZ-X710 microscope (Plan Fluor 10X lens).

Epidermal tongue quantification

Elastin-stained slides were used to perform epidermal tongue quantification. Day 3 images were blinded, and the length of the epidermis beyond the original wound edge, as evidenced by the end of elastin staining, was measured in ImageJ.

Fluorescence detection of MMP-10 activity

The SensoLyte 520 MMP-10 Fluorimetric Assay Kit (AnaSpec) was used to detect MMP-10 activity in wound tissue. Vehicle- or *A. faecalis*–treated murine wounds were prepared, harvested, and cryo-pulverized as described above. In this assay, the MMP-10 substrate is a FRET (fluorescence resonance energy transfer) peptide; therefore, digestion by MMP-10 leads to a fluorescent signal. First, the tissue is incubated with *p*-aminophenylmercuric acetate to activate the MMPs. Then, the tissue is incubated with the MMP-10 substrate for 1 hour at 37°C. Fluorescent signal (relative fluorescence units; RFU) was read at the endpoint. RFU values are reported with background signal subtracted and normalized to the tissue weight added to the reaction.

Statistical analysis

Statistical analyses were performed with the R computing environment (version 4.1.3) and ggplot2 (version 3.3.6) in RStudio (version 2022.02.1+461). For box plots, the center line shows the median value, while the box limits represent the interquartile range (IQR), and whiskers extend up to 1.5 times the IQR. To compare wound sizes of two independent treatment groups from the excisional wounding experiments at a given time point, we performed the Wilcoxon rank sum test. Similarly, gap sizes of two independent treatment groups in the in vitro scratch closure assay were compared with the Wilcoxon rank sum test. The Wilcoxon rank sum test was also used to compare immunofluorescence quantification between two independent treatment groups. For RNA-seq analysis, *P* values were adjusted using the Bonferroni-Hochberg method. *P* values and sample sizes are shown in the main text and figure legends.

Supplementary Materials

This PDF file includes:

Figs. S1 to S5

REFERENCES AND NOTES

1. T. R. Johnson, B. I. Gómez, M. K. McIntyre, M. A. Dubick, R. J. Christy, S. E. Nicholson, D. M. Burmeister, The cutaneous microbiome and wounds: New molecular targets to promote wound healing. *Int. J. Mol. Sci.* **19**, 2699 (2018).
2. E. K. White, E. A. Grice, The wound microbiome. *Cold Spring Harb. Perspect. Biol.* **15**, a041218 (2022).
3. M. Tomic-Canic, J. L. Burgess, K. E. O'Neill, N. Strbo, I. Pastar, Skin microbiota and its interplay with wound healing. *Am. J. Clin. Dermatol.* **21**, 36–43 (2020).
4. C. K. Sen, G. M. Gordillo, S. Roy, R. Kirsner, L. Lambert, T. K. Hunt, F. Gottrup, G. C. Gurtner, M. T. Longaker, Human skin wounds: A major snoballing threat to public health and economy. *Wound Repair Regen.* **17**, 763–771 (2010).
5. S. R. Nussbaum, M. J. Carter, C. E. Fife, J. DaVanzo, R. Haught, M. Nusgart, D. Cartwright, An economic evaluation of the impact, cost, and medicare policy implications of chronic nonhealing wounds. *Value Health* **21**, 27–32 (2018).
6. R. G. Frykberg, J. Banks, Challenges in the treatment of chronic wounds. *Adv. Wound Care* **4**, 560–582 (2015).
7. K. Järbrink, G. Ni, H. Sönnergren, A. Schmidtchen, C. Pang, R. Bajpai, J. Car, The humanistic and economic burden of chronic wounds: A protocol for a systematic review. *Syst. Rev.* **6**, 15 (2017).
8. D. J. Margolis, D. S. Malay, O. J. Hoffstad, C. E. Leonard, T. MaCurdy, Y. Tan, T. Molina, K. L. de Nava, K. L. Siegel, *Economic Burden of Diabetic Foot Ulcers and Amputations: Data Points #3* (Agency for Healthcare Research and Quality, 2011).
9. Canadian Agency for Drugs and Technologies in Health, *Optimal Care of Chronic, Non-Healing, Lower Extremity Wounds: A Review of Clinical Evidence and Guidelines* (Canadian Agency for Drugs and Technologies in Health, 2013).
10. B. R. Freedman, C. Hwang, S. Talbot, B. Hibler, S. Matoori, D. J. Mooney, Breakthrough treatments for accelerated wound healing. *Sci. Adv.* **9**, eade7007 (2023).
11. J. Lukic, V. Chen, I. Strahinic, J. Begovic, H. Lev-Tov, S. C. Davis, M. Tomic-Canic, I. Pastar, Probiotics or pro-healers: The role of beneficial bacteria in tissue repair. *Wound Repair Regen.* **25**, 912–922 (2017).
12. J. S. Meisel, G. Sfyroera, C. Bartow-McKenney, C. Gimblet, J. Bugayev, J. Horwinski, B. Kim, J. R. Brestoff, A. S. Tyldsley, Q. Zheng, B. P. Hodkinson, D. Artis, E. A. Grice, Commensal microbiota modulate gene expression in the skin. *Microbiome* **6**, 20 (2018).
13. A. Uberoi, C. Bartow-McKenney, Q. Zheng, L. Flowers, A. Campbell, S. A. B. Knight, N. Chan, M. Wei, V. Lovins, J. Bugayev, J. Horwinski, C. Bradley, J. Meyer, D. Crumrine, C. H. Sutter, P. Elias, E. Mauldin, T. R. Sutter, E. A. Grice, Commensal microbiota regulates skin barrier function and repair via signaling through the aryl hydrocarbon receptor. *Cell Host Microbe* **29**, 1235–1248.e8 (2021).
14. G. Wang, E. Sweren, H. Liu, E. Wier, M. P. Alphonse, R. Chen, N. Islam, A. Li, Y. Xue, J. Chen, S. Park, Y. Chen, S. Lee, Y. Wang, S. Wang, N. K. Archer, W. Andrews, M. A. Kane, E. Dare, S. K. Reddy, Z. Hu, E. A. Grice, L. S. Miller, L. A. Garza, Bacteria induce skin regeneration via IL-1β signaling. *Cell Host Microbe* **29**, 777–791.e6 (2021).
15. J. Di Domizio, C. Belkhodja, P. Chenuet, A. Fries, T. Murray, P. M. Mondéjar, O. Demaria, C. Conrad, B. Homey, S. Werner, D. E. Speiser, B. Ryffel, M. Gilliet, The commensal skin microbiota triggers type I IFN–dependent innate repair responses in injured skin. *Nat. Immunol.* **21**, 1034–1045 (2020).
16. Y. Lai, A. Di Nardo, T. Nakatsuji, A. Leichtle, Y. Yang, A. L. Cogen, Z. R. Wu, L. V. Hooper, R. R. Schmidt, S. Von Aulock, K. A. Radek, C. M. Huang, A. F. Ryan, R. L. Gallo, Commensal bacteria regulate Toll-like receptor 3-dependent inflammation after skin injury. *Nat. Med.* **15**, 1377–1382 (2009).
17. S. Naik, N. Bouladoux, J. L. Linehan, S. J. Han, O. J. Harrison, C. Wilhelm, S. Conlan, S. Himmelfarb, A. L. Byrd, C. Deming, M. Quinones, J. M. Brenchley, H. H. Kong, R. Tussiwand, K. M. Murphy, M. Merad, J. A. Segre, Y. Belkaid, Commensal–dendritic-cell interaction specifies a unique protective skin immune signature. *Nature* **520**, 104–108 (2015).
18. J. L. Linehan, O. J. Harrison, S. J. Han, A. L. Byrd, I. Vujkovic-Cvijin, A. V. Villarino, S. K. Sen, J. Shaik, M. Smelkinson, S. Tamoutounour, N. Collins, N. Bouladoux, A. Dzutsev, S. P. Rosshart, J. H. Arbuckle, C. R. Wang, T. M. Kristie, B. Rehermann, G. Trinchieri, J. M. Brenchley, J. J. O'Shea, Y. Belkaid, Non-classical immunity controls microbiota impact on skin immunity and tissue repair. *Cell* **172**, 784–796.e18 (2018).
19. O. J. Harrison, J. L. Linehan, H. Y. Shih, N. Bouladoux, S. J. Han, M. Smelkinson, S. K. Sen, A. L. Byrd, M. Enamorado, C. Yao, S. Tamoutounour, F. Van Laethem, C. Hurabielle, N. Collins, A. Paun, R. Salcedo, J. J. O'Shea, Y. Belkaid, Commensal-specific T cell plasticity promotes rapid tissue adaptation to injury. *Science* **363**, eaat6280 (2019).
20. M. G. Constantinides, V. M. Link, S. Tamoutounour, A. C. Wong, P. J. Perez-Chaparro, S. J. Han, Y. E. Chen, K. Li, S. Farhat, A. Weckel, S. R. Krishnamurthy, I. Vujkovic-Cvijin, J. L. Linehan, N. Bouladoux, E. D. Merrill, S. Roy, D. J. Cua, E. J. Adams, A. Bhandoola, T. C. Scharschmidt, J. Aubé, M. A. Fischbach, Y. Belkaid, MAIT cells are imprinted by the microbiota in early life and promote tissue repair. *Science* **366**, eaax6624 (2019).
21. M. Enamorado, W. Kulalert, S. J. Han, I. Rao, J. Delaleu, V. M. Link, D. Yong, M. Smelkinson, L. Gil, S. Nakajima, J. L. Linehan, N. Bouladoux, J. Wlaschin, J. Kabat, O. Kamenyeva, L. Deng, I. Gribonika, A. T. Chesler, I. M. Chiu, C. E. Le Pichon, Y. Belkaid, Immunity to the microbiota promotes sensory neuron regeneration. *Cell* **186**, 607–620.e17 (2023).
22. D. Baltzis, I. Eleftheriadou, A. Veves, Pathogenesis and treatment of impaired wound healing in diabetes mellitus: New insights. *Adv. Ther.* **31**, 817–836 (2014).
23. A. Uberoi, A. Campbell, E. A. Grice, *The Wound Microbiome* (Elsevier, 2020).
24. L. R. Kalan, J. S. Meisel, M. A. Loesche, J. Horwinski, I. Soaita, X. Chen, A. Uberoi, S. E. Gardner, E. A. Grice, Strain- and species-level variation in the microbiome of diabetic wounds is associated with clinical outcomes and therapeutic efficacy. *Cell Host Microbe* **25**, 641–655.e5 (2019).
25. D. Tena, C. Fernáandez, M. R. Lago, Alcaligenes faecalis: An unusual cause of skin and soft tissue infection. *Jpn. J. Infect. Dis.* **68**, 128–130 (2015).
26. N. B. Menke, K. R. Ward, T. M. Witten, D. G. Bonchev, R. F. Diegelmann, Impaired wound healing. *Clin. Dermatol.* **25**, 19–25 (2007).
27. E. C. Bullen, M. T. Longaker, D. L. Updike, R. Benton, D. Ladin, Z. Hou, E. W. Howard, Tissue inhibitor of metalloproteinase-1 is decreased and activated gelatinases are increased in chronic wounds. *J. Invest. Dermatol.* **104**, 236–240 (1995).
28. N. J. Trengove, M. C. Stacey, S. Macauley, N. Bennett, J. Gibson, F. Burslem, G. Murphy, G. Schultz, Analysis of the acute and chronic wound environments: The role of proteases and their inhibitors. *Wound Repair Regen.* **7**, 442–452 (1999).
29. C. Zhang, J. Lim, H. H. Jeon, F. Xu, C. Tian, F. Miao, A. Hameedaldeen, D. T. Graves, FOXO1 deletion in keratinocytes improves diabetic wound healing through MMP9 regulation. *Sci. Rep.* **7**, 10565 (2017).
30. M. J. Reiss, Y. P. Han, E. Garcia, M. Goldberg, H. Yu, W. L. Garner, Matrix metalloproteinase-9 delays wound healing in a murine wound model. *Surgery* **147**, 295–302 (2010).
31. W. Q. Zhang, W. Tang, S. Q. Hu, X. L. Fu, H. Wu, W. Q. Shen, H. L. Chen, Effect of matrix metalloproteinases on the healing of diabetic foot ulcer: A systematic review. *J. Tissue Viability* **32**, 51–58 (2023).
32. M. Muller, C. Trocme, B. Lardy, F. Morel, S. Halimi, P. Y. Benhamou, Matrix metalloproteinases and diabetic foot ulcers: The ratio of MMP-1 to TIMP-1 is a predictor of wound healing. *Diabet. Med.* **25**, 419–426 (2008).
33. D. M. Citron, E. J. C. Goldstein, C. V. Merriam, B. A. Lipsky, M. A. Abramson, Bacteriology of moderate-to-severe diabetic foot infections and in vitro activity of antimicrobial agents. *J. Clin. Microbiol.* **45**, 2819–2828 (2007).
34. K. R. Min, A. Galvis, K. L. B. Nole, R. Sinha, J. Clarke, R. S. Kirsner, D. Ajdic, Association between baseline abundance of Peptoniphilus, a Gram-positive anaerobic coccus, and wound healing outcomes of DFUs. *PLOS ONE* **15**, e0227006 (2020).
35. A. Jnana, V. Muthuraman, V. K. Varghese, S. Chakrabarty, T. S. Murali, L. Ramachandra, K. R. Shenoy, G. S. Rodrigues, S. S. Prasad, D. Dendukuri, A. Morschhauser, J. Nestler, H. Peter, F. F. Bier, K. Satyamoorthy, Microbial community distribution and core microbiome in successive wound grades of individuals with diabetic foot ulcers. *Appl. Environ. Microbiol.* **86**, e02608–e02619 (2020).
36. S. E. Dowd, Y. Sun, P. R. Secor, D. D. Rhoads, B. M. Wolcott, G. A. James, R. D. Wolcott, Survey of bacterial diversity in chronic wounds using pyrosequencing, DGGE, and full ribosome shotgun sequencing. *BMC Microbiol.* **8**, 43 (2008).
37. A. Mahnic, V. Breznik, M. Bombek Ihan, M. Rupnik, Comparison between cultivation and sequencing based approaches for microbiota analysis in swabs and biopsies of chronic wounds. *Front. Med.* **8**, 607255 (2021).
38. T. R. Thomsen, M. S. Aasholm, V. B. Rudkjøbing, A. M. Saunders, T. Bjarnsholt, M. Givskov, K. Kirketerp-Møller, P. H. Nielsen, The bacteriology of chronic venous leg ulcer examined by culture-independent molecular methods. *Wound Repair Regen.* **18**, 38–49 (2010).
39. A. W. Ernlund, L. T. Moffatt, C. M. Timm, K. K. Zudock, C. W. Howser, K. M. Blount, A. Alkhalil, J. W. Shupp, D. K. Karig, Examining the effect of wound cleansing on the microbiome of venous stasis ulcers. *Wound Repair Regen.* **29**, 766–776 (2021).
40. J. Byeon, K. D. Blizinsky, A. Persaud, K. Findley, J. Lee, A. J. Buscetta, S. You, K. Bittinger, C. P. Minniti, V. L. Bonham, E. A. Grice, Insights into the skin microbiome of sickle cell disease leg ulcers. *Wound Repair Regen.* **29**, 801–809 (2021).
41. J. Michaels, S. S. Churgin, K. M. Blechman, M. R. Greives, S. Aarabi, R. D. Galiano, G. C. Gurtner, db/db mice exhibit severe wound-healing impairments compared with other murine diabetic strains in a silicone-splinted excisional wound model. *Wound Repair Regen.* **15**, 665–670 (2007).
42. K. Shettigar, T. S. Murali, Virulence factors and clonal diversity of Staphylococcus aureus in colonization and wound infection with emphasis on diabetic foot infection. *Eur. J. Clin. Microbiol. Infect. Dis.* **39**, 2235–2246 (2020).
43. A. E. Campbell, A. R. McCready-Vangi, A. Uberoi, S. M. Murga-Garrido, V. M. Lovins, E. K. White, J. T. Pan, S. A. B. Knight, A. R. Morgenstern, C. Bianco, P. J. Planet, S. E. Gardner, E. A. Grice. Variable staphyloxanthin production by Staphylococcus aureus drives strain-dependent effects on diabetic wound-healing outcomes. Cell Rep. 42, 113281 (2023).
44. I. Pastar, O. Stojadinovic, N. C. Yin, H. Ramirez, A. G. Nusbaum, A. Sawaya, S. B. Patel, L. Khalid, R. R. Isseroff, M. Tomic-Canic, Epithelialization in wound healing: A comprehensive review. *Adv. Wound Care* **3**, 445–464 (2014).

45. P. Rousselle, F. Braye, G. Dayan, Re-epithelialization of adult skin wounds: Cellular mechanisms and therapeutic strategies. *Adv. Drug Deliv. Rev.* **146**, 344–365 (2019).
46. M. L. Usui, J. N. Mansbridge, W. G. Carter, M. Fujita, J. E. Olerud, Keratinocyte migration, proliferation, and differentiation in chronic ulcers from patients with diabetes and normal wounds. *J. Histochem. Cytochem.* **56**, 687–696 (2008).
47. S. C. S. Hu, C. C. E. Lan, High-glucose environment disturbs the physiologic functions of keratinocytes: Focusing on diabetic wound healing. *J. Dermatol. Sci.* **84**, 121–127 (2016).
48. L. Li, J. Zhang, Q. Zhang, D. Zhang, F. Xiang, J. Jia, P. Wei, J. Zhang, J. Hu, Y. Huang, High glucose suppresses keratinocyte migration through the inhibition of p38 MAPK/autophagy pathway. *Front. Physiol.* **10**, 24 (2019).
49. S. Mazzalupo, M. J. Wawersik, P. A. Coulombe, An ex vivo assay to assess the potential of skin keratinocytes for wound epithelialization. *J Invest. Dermatol.* **118**, 866–870 (2002).
50. M. Krampert, W. Bloch, T. Sasaki, P. Bugnon, T. Rülicke, E. Wolf, M. Aumailley, W. C. Parks, S. Werner, Activities of the matrix metalloproteinase stromelysin-2 (MMP-10) in matrix degradation and keratinocyte organization in wounded skin. *Mol. Biol. Cell* **15**, 5242–5254 (2004).
51. P. Schlage, T. Kockmann, F. Sabino, J. N. Kizhakkedathu, U. Auf Dem Keller, Matrix metalloproteinase 10 degradomics in keratinocytes and epidermal tissue identifies bioactive substrates with pleiotropic functions. *Mol. Cell. Proteomics* **14**, 3234–3246 (2015).
52. U. K. Saarialho-Kere, A. P. Pentland, H. Birkedal-Hansen, W. C. Parks, H. G. Welgus, Distinct populations of basal keratinocytes express stromelysin-1 and stromelysin-2 in chronic wounds. *J. Clin. Invest.* **94**, 79–88 (1994).
53. O. Rechardt, O. Elomaa, M. Vaalamo, K. Pääkkönen, T. Jahkola, J. Höök-Nikanne, R. M. Hembry, L. Häkkinen, J. Kere, U. Saarialho-Kere, Stromelysin-2 is upregulated during normal wound repair and is induced by cytokines. *J. Invest. Dermatol.* **115**, 778–787 (2000).
54. Y. Liu, D. Min, T. Bolton, V. Nubé, S. M. Twigg, D. K. Yue, S. V. M. Lennan, Increased matrix metalloproteinase-9 predicts poor wound healing in diabetic foot ulcers. *Diabetes Care* **32**, 117–119 (2009).
55. G. S. Schultz, A. Wysocki, Interactions between extracellular matrix and growth factors in wound healing. *Wound Repair Regen.* **17**, 153–162 (2009).
56. V. Izzo, M. Meloni, E. Vainieri, L. Giurato, V. Ruotolo, L. Uccioli, High matrix metalloproteinase levels are associated with dermal graft failure in diabetic foot ulcers. *Int. J. Low. Extrem. Wounds* **13**, 191–196 (2014).
57. M. Madlener, C. Mauch, W. Conca, M. Brauchle, W. C. Parks, S. Werner, Regulation of the expression of stromelysin-2 by growth factors in keratinocytes: Implications for normal and impaired wound healing. *Biochem. J.* **320**, 659–664 (1996).
58. N. C. Whittington, S. Wray, Suppression of red blood cell autofluorescence for immunocytochemistry on fixed embryonic mouse tissue. *Curr. Protoc. Neurosci.* **81**, 2.28.1–2.28.12 (2017).
59. J. Bizet, C. Bizet, Strains of Alcaligenes faecalis from clinical material. *J. Infect.* **35**, 167–169 (1997).
60. M. Saghizadeh, D. J. Brown, R. Castellon, M. Chwa, G. H. Huang, J. Y. Ljubimova, S. Rosenberg, K. S. Spirin, R. B. Stolitenko, W. Adachi, S. Kinoshita, G. Murphy, L. J. Windsor, M. C. Kenney, A. V. Ljubimov, Overexpression of matrix metalloproteinase-10 and matrix metalloproteinase-3 in human diabetic corneas: A possible mechanism of basement membrane and integrin alterations. *Am. J. Pathol.* **158**, 723–734 (2001).
61. M. G. Rohani, R. S. McMahan, M. V. Razumova, A. L. Hertz, M. Cieslewicz, S. H. Pun, M. Regnier, Y. Wang, T. P. Birkland, W. C. Parks, MMP-10 regulates collagenolytic activity of alternatively activated resident macrophages. *J. Invest. Dermatol.* **135**, 2377–2384 (2015).
62. B. Fingleton, Matrix metalloproteinases as regulators of inflammatory processes. *Biochim. Biophys. Acta Mol. Cell Res.* **1864**, 2036–2042 (2017).
63. C. Soo, W. W. Shaw, X. Zhang, M. T. Longaker, E. W. Howard, K. Ting, Differential expression of matrix metalloproteinases and their tissue-derived inhibitors in cutaneous wound repair. *Plast. Reconstr. Surg.* **105**, 638–647 (2000).
64. M. A. Moses, M. Marikovsky, J. W. Harper, P. Vogt, E. Eriksson, M. Klagsbrun, R. Langer, Temporal study of the activity of matrix metalloproteinases and their endogenous inhibitors during wound healing. *J. Cell. Biochem.* **60**, 379–386 (1996).
65. O. Stojadinovic, H. Brem, C. Vouthounis, B. Lee, J. Fallon, M. Stallcup, A. Merchant, R. D. Galiano, M. Tomic-Canic, Molecular pathogenesis of chronic wounds: The role of β-catenin and c-myc in the inhibition of epithelialization and wound healing. *Am. J. Pathol.* **167**, 59–69 (2005).
66. D. R. Yager, L. Y. Zhang, H. X. Liang, R. F. Diegelmann, I. K. Cohen, Wound fluids from human pressure ulcers contain elevated matrix metalloproteinase levels and activity compared to surgical wound fluids. *J. Invest. Dermatol.* **107**, 743–748 (1996).
67. A. B. Wysocki, L. Staiano-Coico, F. Grinnell, Wound fluid from chronic leg ulcers contains elevated levels of metalloproteinases MMP-2 and MMP-9. *J. Invest. Dermatol.* **101**, 64–68 (1993).
68. Y. Lai, A. L. Cogen, K. A. Radek, H. J. Park, D. T. MacLeod, A. Leichtle, A. F. Ryan, A. Di Nardo, R. L. Gallo, Activation of TLR2 by a small molecule produced by staphylococcus epidermidis increases antimicrobial defense against bacterial skin infections. *J. Invest. Dermatol.* **130**, 2211–2221 (2010).
69. A. M. O'Neill, T. Nakatsuji, A. Hayachi, M. R. Williams, R. H. Mills, D. J. Gonzalez, R. L. Gallo, Identification of a human skin commensal bacterium that selectively kills Cutibacterium acnes. *J. Invest. Dermatol.* **140**, 1619–1628.e2 (2020).
70. T. Nakatsuji, T. H. Chen, S. Narala, K. A. Chun, A. M. Two, T. Yun, F. Shafiq, P. F. Kotol, A. Bouslimani, A. V. Melnik, H. Latif, J. N. Kim, A. Lockhart, K. Artis, G. David, P. Taylor, J. Streib, P. C. Dorrestein, A. Grier, S. R. Gill, K. Zengler, T. R. Hata, D. Y. M. Leung, R. L. Gallo, Antimicrobials from human skin commensal bacteria protect against Staphylococcus aureus and are deficient in atopic dermatitis. *Sci. Transl. Med.* **9**, eaah4680 (2017).
71. A. L. Cogen, K. Yamasaki, J. Muto, K. M. Sanchez, L. C. Alexander, J. Tanios, Y. Lai, J. E. Kim, V. Nizet, R. L. Gallo, Staphylococcus epidermidis antimicrobial δ-toxin (phenol-soluble modulin-γ) cooperates with host antimicrobial peptides to kill group A Streptococcus. *PLOS ONE* **5**, e8557 (2010).
72. A. Zipperer, M. C. Konnerth, C. Laux, A. Berscheid, D. Janek, C. Weidenmaier, M. Burian, N. A. Schilling, C. Slavetinsky, M. Marschal, M. Willmann, H. Kalbacher, B. Schittek, H. Brötz-Oesterhelt, S. Grond, A. Peschel, B. Krismer, Human commensals producing a novel antibiotic impair pathogen colonization. *Nature* **535**, 511–516 (2016).
73. A. M. Nelson, S. K. Reddy, T. S. Ratliff, M. Z. Hossain, A. S. Katseff, A. S. Zhu, E. Chang, S. R. Resnik, C. Page, D. Kim, A. J. Whittam, L. S. Miller, L. A. Garza, dsRNA released by tissue damage activates TLR3 to drive skin regeneration. *Cell Stem Cell* **17**, 139–151 (2015).
74. S. Liu, Y. H. Hur, X. Cai, Q. Cong, Y. Yang, C. Xu, A. M. Bilate, K. A. U. Gonzales, S. M. Parigi, C. J. Cowley, B. Hurwitz, J.-D. Luo, T. Tseng, S. Gur-Cohen, M. Sribour, T. Omelchenko, J. Levorse, H. A. Pasolli, C. B. Thompson, D. Mucida, E. Fuchs, A tissue injury sensing and repair pathway distinct from host pathogen defense. *Cell* **186**, 2127–2143.e22 (2023).
75. B. A. Lipsky, A. R. Berendt, P. B. Cornia, J. C. Pile, E. J. G. Peters, D. G. Armstrong, H. G. Deery, J. M. Embil, W. S. Joseph, A. W. Karchmer, M. S. Pinzur, E. Senneville, 2012 Infectious Diseases Society of America clinical practice guideline for the diagnosis and treatment of diabetic foot infections. *Clin. Infect. Dis.* **54**, e132–e173 (2012).
76. L. Kalan, M. Loesche, B. P. Hodkinson, K. Heilmann, G. Ruthel, S. E. Gardner, E. A. Grice, Redefining the chronic-wound microbiome: Fungal communities are prevalent, dynamic, and associated with delayed healing. *MBio* **7**, e01058-16 (2016).
77. M. Loesche, S. E. Gardner, L. Kalan, J. Horwinski, Q. Zheng, B. P. Hodkinson, A. S. Tyldsley, C. L. Franciscus, S. L. Hillis, S. Mehta, D. J. Margolis, E. A. Grice, Temporal stability in chronic wound microbiota is associated with poor healing. *J. Invest. Dermatol.* **137**, 237–244 (2017).
78. N. S. Levine, R. B. Lindberg, A. D. J. Mason, B. A. J. Pruitt, The quantitative swab culture and smear: A quick, simple method for determining the number of viable aerobic bacteria on open wounds. *J. Trauma* **16**, 89–94 (1976).
79. J. Versalovic, K. C. Carroll, G. Funke, J. H. Jorgensen, M. L. Landry, D. W. Warnock, *Manual of Clinical Microbiology* (ASM Press, 2011).
80. D. T. Truong, E. A. Franzosa, T. L. Tickle, M. Scholz, G. Weingart, E. Pasolli, A. Tett, C. Huttenhower, N. Segata, MetaPhlAn2 for enhanced metagenomic taxonomic profiling. *Nat. Methods* **12**, 902–903 (2015).
81. M. Gao, T. T. Nguyen, M. A. Suckow, W. R. Wolter, M. Gooyit, S. Mobashery, M. Chang, Acceleration of diabetic wound healing using a novel protease-anti-protease combination therapy. *Proc. Natl. Acad. Sci. U.S.A.* **112**, 15226–15231 (2015).
82. F. Li, C. A. Adase, L. J. Zhang, Isolation and culture of primary mouse keratinocytes from neonatal and adult mouse skin. *J. Vis. Exp.* **2017**, 56027 (2017).
83. A. Suarez-Arnedo, F. T. Figueroa, C. Clavijo, P. Arbeláez, J. C. Cruz, C. Muñoz-Camargo, An image J plugin for the high throughput image analysis of in vitro scratch wound healing assays. *PLOS ONE* **15**, e0232565 (2020).
84. A. Salic, T. J. Mitchison, A chemical method for fast and sensitive detection of DNA synthesis in vivo. *Proc. Natl. Acad. Sci. U.S.A.* **105**, 2415–2420 (2008).
85. B. E. Keyes, S. Liu, A. Asare, S. Naik, J. Levorse, L. Polak, C. P. Lu, M. Nikolova, H. A. Pasolli, E. Fuchs, Impaired epidermal to dendritic t cell signaling slows wound repair in aged skin. *Cell* **167**, 1323–1338.e14 (2016).
86. S. Andrews, FastQC, https://www.bioinformatics.babraham.ac.uk/projects/fastqc/.
87. N. L. Bray, H. Pimentel, P. Melsted, L. Pachter, Near-optimal probabilistic RNA-seq quantification. *Nat. Biotechnol.* **34**, 525–527 (2016).
88. C. Soneson, M. I. Love, M. D. Robinson, Differential analyses for RNA-seq: Transcript-level estimates improve gene-level inferences. *F1000Res.* **4**, 1521 (2015).
89. M. I. Love, W. Huber, S. Anders, Moderated estimation of fold change and dispersion for RNA-seq data with DESeq2. *Genome Biol.* **15**, 550 (2014).
90. Y. Benjamini, Y. Hochberg, Controlling the false discovery rate: A practical and powerful approach to multiple testing. *J. R. Stat. Soc. Ser. B.* **57**, 289–300 (1995).
91. L. Kolberg, U. Raudvere, I. Kuzmin, J. Vilo, H. Peterson, gprofiler2—An R package for gene list functional enrichment analysis and namespace conversion toolset g:Profiler. *F1000Res.* **9**, ELIXIR-709 (2020).

Acknowledgments: We would like to thank the Penn Skin Biology and Diseases Resource-based Center CPAT and STAR cores for their invaluable assistance with histopathology and provision of skin samples. In particular, we thank J. Seykora, S. Prouty, and T. Dentchev for their expert histological processing, staining, and interpretations of pathology and quality. We would also like to thank the Children's Hospital of Philadelphia High Throughput Sequencing

Core for their support of the RNA-seq experiment. We are very grateful to current and former members of the Grice Lab and the Department of Dermatology for critical discussion and review of the work. We would like to thank the clinical staff at the University of Pennsylvania and University of Iowa for assistance with patient sample collection as well as the patients who generously participated in the study. We thank D. Lee, McArdle Laboratory for Cancer Research, University of Wisconsin-Madison for sharing details of home-based protocol for measuring EdU incorporation. Parts of the conceptual figures were created with BioRender.com. **Funding:** This work was supported by the NIH National Institute of Nursing Research [R01NR009448 (S.E.G.)], NIH National Institute of Nursing Research [R01NR015639 (E.A.G.)], NIH National Institute of Arthritis and Musculoskeletal and Skin Diseases [P30AR069589 (E.A.G.)], NIH National Institute of Arthritis and Musculoskeletal and Skin Diseases [F31AR079852 (E.K.W.)], NIH National Institute of Arthritis and Musculoskeletal and Skin Diseases [T32AR007465 (E.K.W. and J.C.H.)], Prevent Cancer Foundation Awesome Games Done Quick fellowship (A.U.), NIH National Institute of Arthritis and Musculoskeletal and Skin Diseases [K99 AR081404 (A.U.)], Penn SBDRC Pilot and Feasibility Grant [P30AR069589 (A.U.)], Penn Blavatnik Family Fellowship (A.C.), NIH National Institute of Arthritis and Musculoskeletal and Skin Diseases [F31AR079845 (J.C.H.)], NIH National Institute of Allergy and Infectious Diseases [5T32AI141393 (M.W.)], and NIH National Institute of General Medical Sciences [R25 GM071745-19 (N.Y.R.)]. **Author contributions:** Conceptualization: E.K.W., A.U., J.T.-C.P., M.W., S.E.G., and E.A.G. Methodology: E.K.W., A.U., J.T.-C.P., J.T.O., A.E.C., M.W., and S.E.G. Resources: E.K.W., S.E.G., and E.A.G. Funding acquisition: E.K.W., S.E.G., and E.A.G. Investigation: E.K.W., A.U., J.T.-C.P., J.T.O., A.E.C., S.M.M.-G., J.C.H., M.W., N.Y.R., and S.E.G. Software: A.E.C. Visualization: E.K.W., A.U., A.E.C., and E.A.G. Validation: E.K.W., A.U., J.P., S.M.M.-G., and M.W. Supervision: E.K.W. and E.A.G. Data curation: A.E.C. and S.E.G. Formal analysis: E.K.W., A.U., A.E.C., and P.B. Project administration: E.K.W., J.T.-C.P., and E.A.G. Writing—original draft: E.K.W. and A.U. Writing—review and editing: E.K.W., S.M.M.-G., A.E.C., M.W., S.E.G., and E.A.G. **Competing interests:** The authors declare that they have no competing interests. **Data and materials availability:** All data needed to evaluate the conclusions in the paper are present in the paper and/or the Supplementary Materials. The RNA-seq dataset generated and analyzed in this study is publicly available for download in the National Center for Biotechnology Information Gene Expression Omnibus (GEO GSE261418).

Submitted 29 June 2023
Accepted 20 May 2024
Published 26 June 2024
10.1126/sciadv.adj2020